The Thesis Committee for Christopher Conway Easterby
Certifies that this is the approved version of the following Thesis:

CFD Evaluation of Internal Flow Effects on Turbine Blade Leading-Edge Film Cooling and Overall Cooling with Shaped Hole Geometries

APPROVED BY
SUPERVISING COMMITTEE:

David Bogard, Supervisor

Todd Oliver

CFD Evaluation of Internal Flow Effects on Turbine Blade Leading-Edge Film Cooling and Overall Cooling with Shaped Hole Geometries

by

Christopher Conway Easterby

Thesis

Presented to the Faculty of the Graduate School of

The University of Texas at Austin

in Partial Fulfillment

of the Requirements

for the Degree of

Master of Science in Engineering

The University of Texas at Austin

May 2021

Acknowledgements

There are many who deserve immense thanks for helping me along the path of my academic journey so far, especially in the process of completing my master's degree.

First, Dr. Bogard has been the greatest advisor I could have asked for. He welcomed me into the lab a little over a year ago and I have since learned more than I thought possible in such a short time. His expertise on turbine cooling, advise on engineering and life in general, and insights into predicting football scores have all been invaluable. I can certainly say I owe much of my current opportunities to him. I am also extremely thankful to Dr. Oliver for the feedback on this thesis and advice in creating the computational model.

Despite having very limited face-to-face interactions (due to the entirety of my time in the lab taking place during a global pandemic), the other graduate students in the lab have also been crucial to my success for the past year and a half. Although I was joining the lab as they were finishing, Jacob and Fraser were instrumental in the development of this thesis thanks to Jacob's dissertation (on which this thesis was based) and Fraser's help learning CFD techniques. Dale has been another great source of advice as well as a pleasure to work with on the GOALI project and Matt, Chris and Michael contributed substantially to my understanding of turbine cooling and CFD.

I must also thank the University of Texas at Austin for being such an outstanding place to learn and grow. The last 6 years here have been unforgettable and made me who I am now.

Lastly, huge thanks are in order for my friends and family. My mom and dad have been so important in giving me the opportunity to learn as much as I have, offering limitless advice, and literally supporting me since day one. My younger brother Will deserves a shoutout as well, for always being a friend and occasionally helping me fix a computer issue. The rest of my family, from grandparents to aunts, have also played a huge role in my opportunities and I thank them greatly for that. Last, but certainly not least, I am so grateful for Elizabeth, who has been there to offer the strongest of support since my undergraduate years. Thank you all so much and I love all of you.

Abstract

CFD Evaluation of Internal Flow Effects on Turbine Blade Leading-Edge Film Cooling and Overall Cooling with Shaped Hole Geometries

Christopher Conway Easterby, M.S.E.

The University of Texas at Austin, 2021

Supervisor: David Bogard

In gas turbine engines, the highest heat loads occur at the leading-edge areas of turbine blades and vanes. To protect the blades and vanes, a "showerhead" configuration of film cooling holes is often used for this location, in which several rows of holes are configured closely together to maximize film coverage. Typically, these film cooling holes are fed by impingement cooling jets, helping to cool the leading edge internally, but also changing the internal flow field. The effects of these internal flow fields on film cooling are not well known, and experimental research is very limited in its ability to analyze them. Because of this, computational fluid dynamic (CFD) simulations using RANS were used as a way to analyze these internal flow fields. To isolate the effects of the impingement jet, results were compared to a pseudo-plenum internal feed, and rotation in the hole caused by the impingement was found to be a key factor in performance. Computational results from both coolant feed configurations were compared to experimental results for the same configurations. The CFD RANS results were found to follow the same trends as the

experimental results for both the impingement-fed and plenum-fed cases, suggesting that RANS is able to accurately model some of the important physics associated with leading-edge film cooling. Additionally, the effects of the impingement feed on overall cooling effectiveness were analyzed and found to be significant at lower blowing ratios but less significant at higher blowing ratios.

Table of Contents

List of Tables

List of Figures

Chapter 1: Introduction[1]

This section covers the various turbine blade cooling concepts necessary for understanding the concepts studied in this thesis. This includes general film cooling, leading-edge film cooling, shaped film cooling holes, internal coolant feeds, and computational approaches for studying turbine blade cooling.

1.1 Turbine Blade/Vane Cooling

As the highest temperatures in gas turbine engines increase to meet greater efficiency and performance demands, so too does the need for effective cooling of the turbine blades to prevent damage from the high temperature combustion gases. Conventional turbine blade cooling uses the cooler pressurized air from the compressor, which bypasses the combustor. From there, two major types of cooling can be used. Internal cooling involves running the cool air through interior passages in the blades designed to maximize heat transfer with the blade, while external cooling involves ejecting the cool air onto the surface of the blade to form a protective film acting as a barrier from the hot mainstream air. This technique is referred to as film cooling and is often used in conjunction with internal cooling at the blade areas which experience the highest heat loads [1].

Some of the key parameters involved in turbine cooling which are discussed in this study include density ratio (DR) and blowing ratio (M), defined below.

---

[1]Includes material previously published in:
Easterby, Christopher C, Moore, Jacob D and Bogard, David G. "CFD Evaluation of Internal Flow Effects on Turbine Blade Leading-Edge Film Cooling with Shaped Hole Geometries." *Proceedings of the ASME Turbo Expo*. GT2021-59780. Online, June 7–11, 2021.
The author of the current thesis was the lead author for this paper.

$$DR = \frac{\rho_c}{\rho_\infty} \tag{1.1}$$

$$M = \frac{\rho_c U_c}{\rho_\infty U_\infty} \tag{1.2}$$

Here, ρ_c is the density of the coolant, ρ_∞ is the density of the mainstream gas, U_c is the average coolant velocity in the metering section of the hole, and U_∞ is the mainstream approach velocity. These non-dimensional parameters are used for scaling in studies.

Adiabatic effectiveness (η) and non-dimensional thermal field temperature (θ) are also defined below.

$$\eta = \frac{T_\infty - T_{aw}}{T_\infty - T_{c,exit}} \tag{1.3}$$

$$\theta = \frac{T_\infty - T}{T_\infty - T_c} \tag{1.4}$$

Here, T_∞ is the mainstream approach temperature, T_{aw} is the surface temperature of a theoretical adiabatic blade, $T_{c,exit}$ is the temperature of the coolant at the exit of the hole, and T_c is the off-wall temperature of the coolant or the mainstream gases at specified locations. Adiabatic effectiveness is a non-dimensional surface temperature used to study film cooling performance isolated from conduction cooling, while θ is used for off-wall thermal field measurements.

1.1.1 Leading-Edge Film Cooling

The section of the blades (and vanes) which experiences the highest heat load is the leading edge, near the stagnation point of the blade. This means that these areas require the most effective cooling, and showerhead film cooling is one of the most

common techniques used for this. Showerhead film cooling for leading-edge regions involves using a tightly packed array of holes (resembling a showerhead), often in rows offset from each other, to maximize the coverage of the coolant on the leading edge. Figure 1.1 below illustrates a typical showerhead arrangement of film cooling holes for a blade leading edge, as well as some of the most common terminology used in the showerhead region.

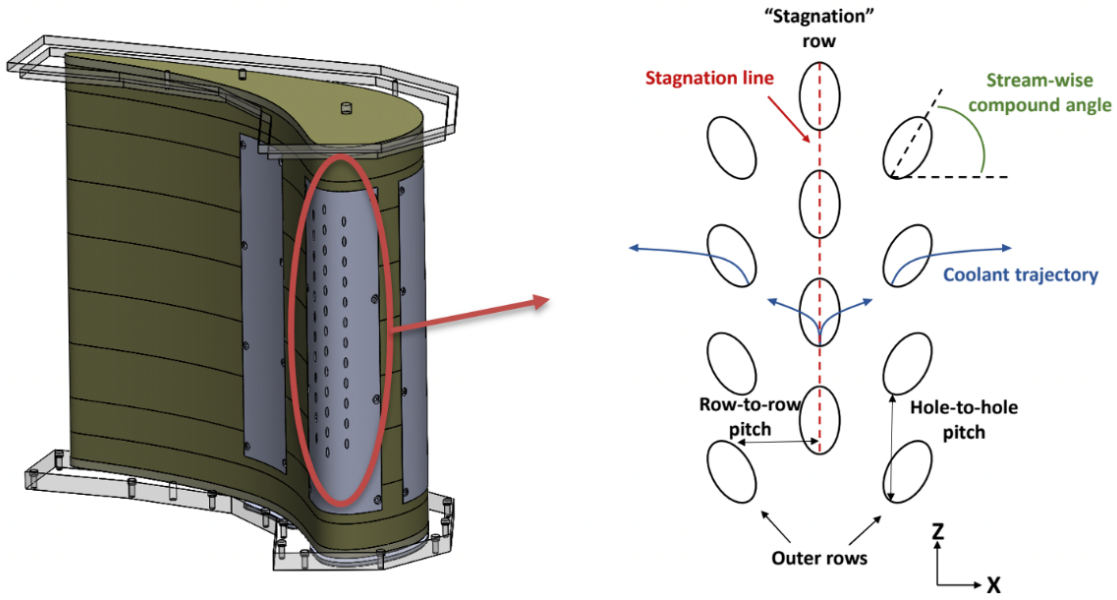

Figure 1.1: Typical Leading-Edge Showerhead Film Cooling Hole Arrangement [12]

Film cooling studies in this region are limited, and studies that focus on film cooling in locations downstream of the leading edge (such as flat plate experiments) may not capture the physics involved in the leading-edge flow fields. Some of the main factors which must be considered for leading-edge film cooling are the curvature of the blade

surface, the internal coolant feeds used at the leading edge, and the impingement of the mainstream gases at the stagnation row on the leading edge. Overall, leading-edge film cooling is a unique problem to consider in turbine cooling, and conclusions drawn using other configurations may not apply [2].

1.1.2 Shaped Hole Film Cooling

One important area of film cooling improvement has come from shaped film cooling holes [3-5]. These holes are shaped differently than conventional cylindrical holes and designed to more effectively diffuse and spread the coolant, encouraging better film coverage and thus better cooling performance. Previous studies have looked into a variety of different shapes and their effectiveness. Figure 1.2 below shows some of the most common shapes compared to a conventional cylindrical hole.

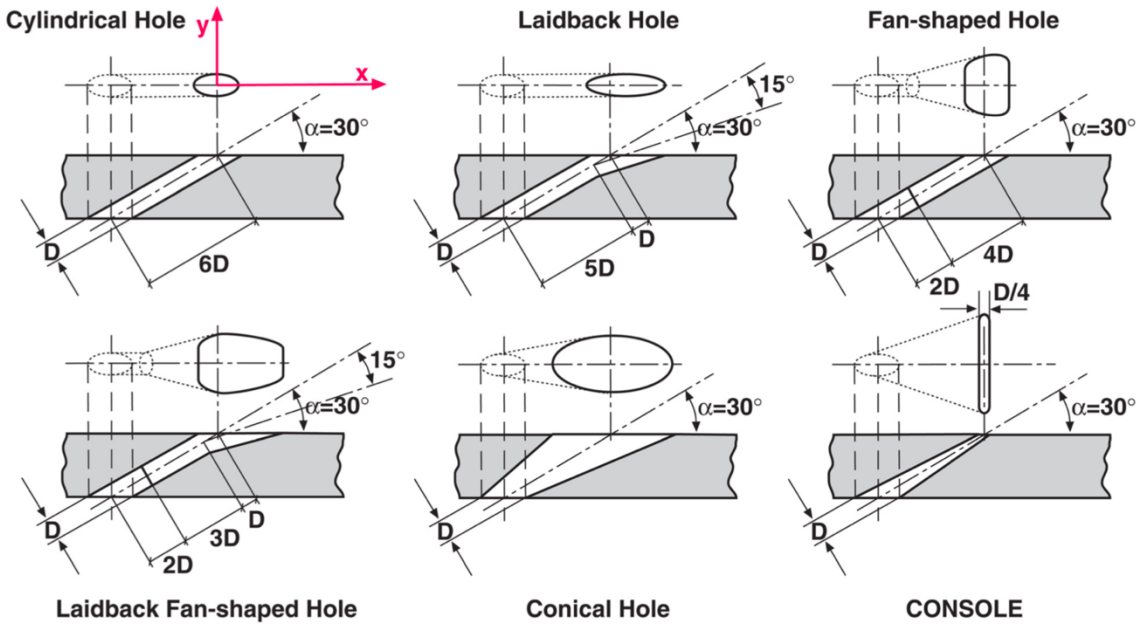

Figure 1.2: Shaped Hole Examples [13]

This study will focus on conical shaped holes, which are often defined using expansion angle (α), shown above in Figure 1.2, and area ratio (AR), defined below.

$$AR = \frac{A_{shape}}{A_{meter}} \tag{1.5}$$

Here, A_{shape} is the cross-sectional area of the hole at the outlet and A_{meter} is the cross-sectional area of the initial metering section of the hole. Conical holes were chosen for the purpose of comparison with an experimental conical hole study performed previously by Moore [5].

1.2 Internal Flow Effects in the Leading Edge

One important aspect of leading-edge film cooling which differentiates it from simpler configurations is the type of internal coolant feed. Generally, the showerhead holes are fed by a coolant jet which impinges on the internal surface of the leading edge and then moves along the surface to the inlets of the holes. This impingement provides some additional cooling of the blade via cooling of the internal surface, but also affects the way in which coolant flows through the film cooling holes. Because of this, the behavior of the coolant exiting the holes can be changed and thus the film cooling performance affected. This feed is sometimes simplified experimentally for isolated film cooling studies by using a "pseudo-plenum" feed designed to simulate a plenum in which no internal flow effects are present, but limited literature has suggested this simplification may significantly impact film cooling performance [2]. Unfortunately, experimental studies are limited in their

ability to analyze these affects, since access to the interior of experimental blade models is generally highly restricted.

1.3 Computational Cooling Analysis

A promising method for analyzing the internal flow effects further is computational fluid dynamics (CFD) simulation which allows for thorough examination of the blade interior. This method has several well-documented issues (discussed further in section 2) but has shown potential for modelling some of the key aspects of leading-edge film cooling, especially when validated against experimental data. The effectiveness of CFD simulation can vary significantly, with techniques such as large eddy simulation (LES) showing the ability to very effectively model film cooling. However, the extensive computational resources required for this technique generally lead to studies which use less computationally expensive but less accurate methods such as Reynolds-averaged Navier-Stokes (RANS). Still, these more feasible methods have shown reasonable accuracy for turbine blade cooling studies, discussed further in section 1.4.3.

1.4 Literature Review

This section reviews literature relevant to the present study. This includes leading-edge shaped hole film cooling studies, leading-edge internal flow field studies, and leading-edge film cooling computational studies.

1.4.1 Leading-Edge Shaped Hole Film Cooling Studies

Literature on shaped hole film cooling in the leading-edge showerhead region is currently limited. While shaped hole flat plate studies have become more common, other studies which looked at leading-edge showerhead film cooling almost all focused on cylindrical holes. However, it has recently become more feasible to test shaped holes, and several studies have done so experimentally with leading-edge blade models. Reiss and Bölcs found that conically shaped holes with an expansion angle of 15 degrees and an area ratio of 1.5 performed significantly better than cylindrical holes in terms of adiabatic effectiveness across all blowing ratios for a leading-edge vane model, with improvements of 30-40% [3].

Another study by Gao and Han that tested a blade leading-edge model with three rows of holes also found that conically shaped holes with a 5-degree expansion angle and $AR = 1.9$ performed significantly better than cylindrical holes, particularly at higher blowing ratios where performance was again improved by 30-40% [4].

The study by Moore [5] which this thesis attempted to simulate computationally also found a significant increase in cooling performance across blowing ratios ranging from $M = 0.50$ to $M = 3.1$ when conically shaped holes were used in the showerhead region in place of cylidrical holes, with performance increasing from 20% to 100% depending on the blowing ratio and location. This increase in performance was found to come primarily from the better attachment of the coolant jets to the blade surface that these shaped holes allowed. This study tested two different area ratios ($AR = 2.5$ and $AR = 3.5$) and expansion angles (7 degrees and 12 degrees) and found that the best

performing holes had $AR = 3.5$ and an expansion angle of 7 degrees, though the differences between the performances of the shaped holes were small (10-15%) relative to the large variation of the parameters.

Overall, shaped hole leading-edge film cooling studies are limited but the studies that do exist suggest a significance performance increase when conical holes are used in place of cylindrical holes. The ideal area ratios and expansion angles of these holes are not well documented, but the study by Moore suggested these parameters do not significantly impact performance due to the positive correlation between AR and performance, the negative correlation between α and performance, and the fact that increasing AR inherently increases α [5].

1.4.2 Internal Flow Effect Studies

One factor in leading-edge shaped hole film cooling which has very rarely been studied is the effect of the internal flow fields in the blade. Experimental research is highly limited in its ability to analyze these internal flow fields, as the interior of the blade is generally inaccessible during tests.

The study mentioned previously by Moore [5] attempted to analyze these flow field effects by comparing the film cooling performance on a leading-edge showerhead blade model with a conventional impingement feed to the performance on the same model with a pseudo-plenum coolant feed, designed to minimize the internal flow effects. This study was performed with an adiabatic blade model to isolate film cooling effects. They found that there were significant differences between the two cases, with

differences in adiabatic effectiveness of approximately 10-15% in the near-hole areas. While the performance for the pressure side holes was similar for the different feed designs, the row of holes on the suction side of the leading edge at higher blowing ratios ($M = 2.32$ and $M = 3.1$) saw significantly higher performance for the impingement feed than the plenum feed. For these suction side holes, the coolant remained attached much more effectively with an impingement feed than with a plenum feed.

While this study attempted to measure the effects of the impingement feed on only film cooling, several studies have measured the effects of an impingement feed on overall cooling effectiveness, including internal and bore cooling effects. Mouzon et al. interestingly found negligible effects on overall cooling with the addition of an impingement feed at $M = 2.0$, despite a doubling of the internal heat transfer coefficient [6]. A follow-up study by Ravelli et al. investigated these effects computationally and confirmed the findings [7]. This study revealed that the reason for these results was the fact that most of the additional cooling comes from bore cooling (caused by the coolant flowing through the holes) and not from cooling of the internal chamber surface.

Overall, while some studies have analyzed the effects of internal feeds on overall cooling, there is very little insight into the isolated effects of internal feeds on film cooling performance.

1.4.3 Computational Studies

An option which allows more thorough analysis of the internal flow fields is CFD simulation. While current CFD simulation techniques almost always come with some

amount of error, several studies have shown the ability to predict many of the key physics associated with leading-edge film cooling.

One study by Ravelli and Barigozzi used RANS CFD to predict leading-edge showerhead film cooling with cylindrical holes using a realizable $k-\varepsilon$ (RKE) turbulence model and an SST $k-\omega$ turbulence model which were compared to experimental results [8]. The study found that the RANS computation was able to predict many of the key flow characteristics well, with the RKE model achieving results more closely matching experimental results than the SST model due to its better prediction of coolant jet attachment and the trends of adiabatic effectiveness versus blowing ratio. Areas near the holes were found to have the strongest similarities between the CFD and experimental results. However, it was also found that there were sometimes significant errors in the predictions for both computational models, especially in the prediction of coolant-mainstream mixing and occasionally in the prediction of coolant jet attachment. These issues were found to become more significant as blowing ratio increased and caused poor predictions in areas downstream of the holes.

Another study by Zhang et al. used RANS with an RKE turbulence model to simulate film cooling performance for a leading-edge configuration with shaped holes and compared the results to experimental measurements [9]. This study found similar results, with the RANS RKE results showing good agreement with the experimental results in areas near the stagnation row and poor agreement in areas further downstream. In these downstream areas, the underprediction of coolant dispersion due to mainstream

mixing was found to cause overpredictions of adiabatic effectiveness of approximately 30%.

While studies using CFD to simulate leading-edge showerhead cooling exist, the results were almost all obtained with cylindrical holes, with the Zhang et al. study being the only to look at shaped hole leading-edge configurations, and the internal feed effects on film cooling were not considered.

1.5 PRESENT STUDY

This study attempted to validate the promise seen by Zhang et al. [9] in the ability of RANS CFD to model key characteristics of leading-edge film cooling by comparing computational results to experimental results obtained by Moore [5] using the same setup. It also more thoroughly examined the internal flow effects on leading-edge film cooling by taking computational results with a conventional impingement feed and comparing them to results taken with a pseudo-plenum feed, designed to negate internal flow effects. These results utilized an adiabatic blade model to isolate film cooling effects and sought to explain the difference in performance seen experimentally by Moore between impingement-fed and plenum-fed cases on the suction side of the blade at $M = 3.1$. This analysis was done by examination of the effects the impingement feed has on the coolant flow fields through the holes, particularly how the coolant exits the holes. Lastly, the effects of the internal flow fields on overall leading-edge cooling (including film cooling and internal convection cooling) were examined using a blade model designed to match the Biot number present in real engine conditions.

Chapter 2: Computational Setup[2]

In this section, the various aspects of setting up the computational study are reviewed. This includes the computational blade models, the computational domain for simulation, the mesh used, and the setup of the simulation itself.

2.1 Blade Models

Two CAD models of a turbine blade were first created to be used in the CFD simulation. These models were designed to match those used in the previously mentioned experimental study by Moore [5], which used a blade geometry adapted from Kopriva et al. [10]. The model is a scaled-up version of a turbine blade with a scaling factor of x15.5, resulting in a blade chord length of 602 mm and an axial chord length of 474 mm. It also includes an internal coolant chamber behind the leading edge to interface between the coolant piping and the showerhead holes.

The showerhead incorporates the configuration of shaped holes at the leading edge, with one row at the stagnation line of the blade, a second row $6D$ downstream on the suction side, and a third row $6D$ downstream on the pressure side. The suction side row and pressure side row are both laterally offset from the stagnation row by half of the hole-to-hole pitch, which is $6D$. Figure 2.1 shows these rows. All holes are at a 30-degree injection angle to the surface and a 90-degree angle to the freestream flow. The metering section of all holes has a hole diameter of $D = 4.7$ mm, and the shaping of the holes is

[2]Includes material previously published in:
Easterby, Christopher C, Moore, Jacob D and Bogard, David G. "CFD Evaluation of Internal Flow Effects on Turbine Blade Leading-Edge Film Cooling with Shaped Hole Geometries." *Proceedings of the ASME Turbo Expo*. GT2021-59780. Online, June 7–11, 2021.
The author of the current thesis was the lead author for this paper.

designed to match that of the most effective shaped holes from Moore's study [5], with an area ratio of 3.5 and an expansion angle of 7-degrees.

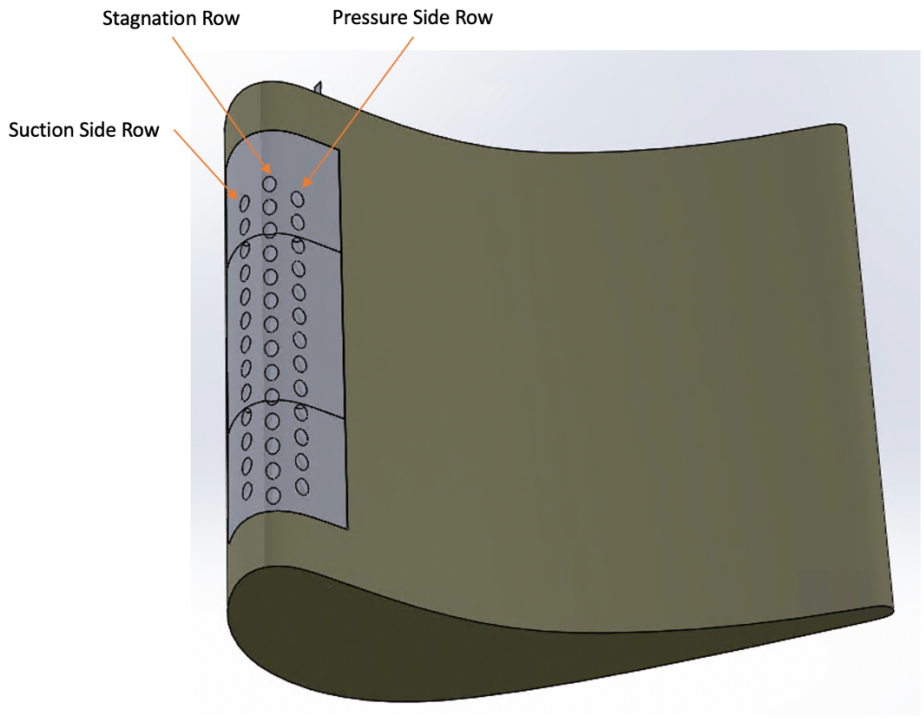

Figure 2.1: Position of Rows in Showerhead for Computational Model

The two CAD models were identical for the blade and showerhead but differed in their internal coolant feed design. The first model was designed to replicate an internal impingement feed and consisted of a cylindrical pipe inside of the interior coolant chamber with a row of holes directed towards the back surface of the leading edge. This pipe was used experimentally to act as an interface between the coolant piping and the coolant chamber. The second model was designed to simulate a plenum for the coolant chamber, where flow field effects are negligible. It consisted of the same pipe, but with a

row of holes directed at the back of the coolant chamber (opposite of the leading edge) such that the flow from the pipe impinged on the surface away from the leading edge and was more slowly diffused to the film cooling hole inlets. Figure 2.2 shows the CAD models.

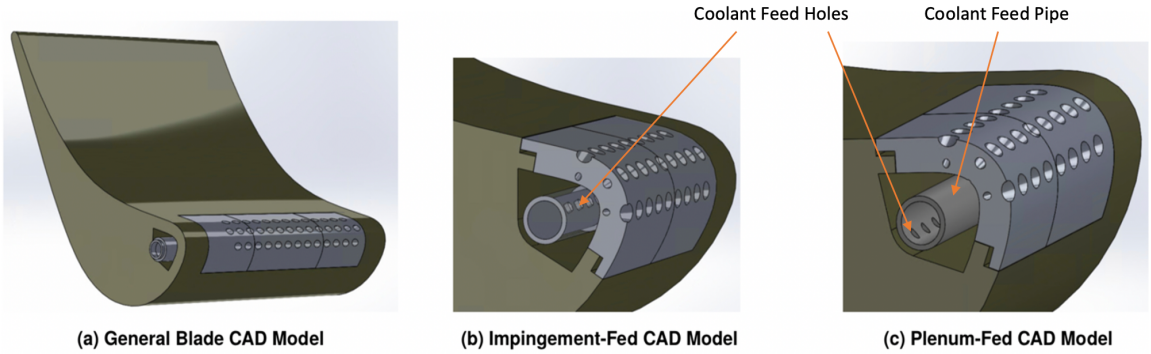

Figure 2.2: CAD Models

2.2 Computation Domain

The computational domain for simulation was created to maximize the possible resolution of the mesh (given computational limits), while also capturing all of the important flow field features. Because the experimental results from Moore [5] showed periodic behavior, this was done using periodic conditions. The span of the blade domain used was one hole-to-hole pitch, meaning the pressure side and suction side holes were cut in half. A spanwise periodic boundary condition was imposed on all surfaces to allow modelling of the entire blade. The outer fluid body was made to model an infinite cascade of blades, such that the mainstream flow inlet (shown on the left side of Figure 2.3b) was

one blade-to-blade pitch away from the tip of the leading edge, the mainstream flow outlet (shown on the right side of Figure 2.3b) was one blade-to-blade pitch away from the tip of the trailing edge, and the distance from the top of the domain to the bottom (as shown in Figure 2.3b) was one blade-to-blade pitch with a periodic repeat condition imposed. The blade-to-blade pitch used was the same as that used in the experiments by Moore [5] at 445 mm. Figure 2.3 shows both domains.

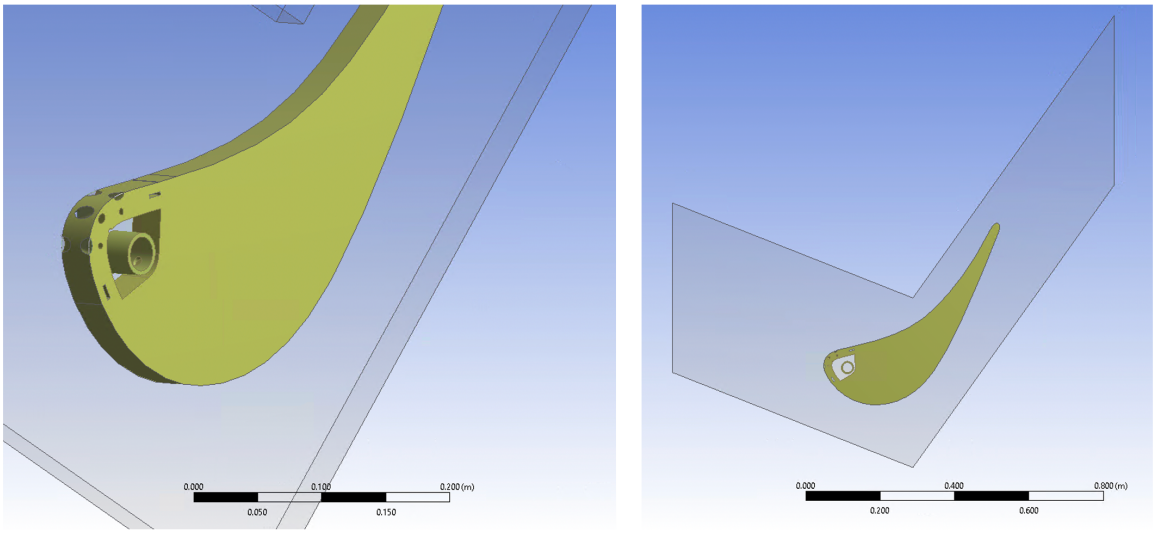

a) Blade Domain **b) Fluid Domain**

Figure 2.3: Computational Domains

2.3 MESH

The mesh was created for simulation using the CAD models and the meshing tool in Ansys Workbench. The mesh was designed to achieve accurate results by ensuring the variables of interest were independent of the mesh features.

2.3.1 Description of Mesh

Both the solid and fluid bodies in the model were meshed such that conjugate heat transfer studies could be performed. For the bulk areas of the fluid and solid bodies, a uniform mesh element size of $0.4D$ (2.1 mm) was used. To account for the finer aspects of flow and heat transfer close to the walls, inflation regions were created in the fluid body near the walls. These inflation regions were created by using a total thickness of $3D$ (14 mm) with 30 inflation layers in this $3D$ thickness. The thickness of the region was chosen such that it would encompass the boundary layers and the coolant jets from the film cooling holes in all areas of the leading-edge. The $3D$ thickness ensured that even the coolant jets which showed a high degree of separation from the blade surface (such as those at higher blowing ratios) would be fully within the inflation region. It was observed that this was important to accurately model cooling performance for such jets, discussed further in section 2.3.3. The number of layers within the region was chosen such that the near wall y+ values would be less than or equal to 1, as required by the turbulence model used. Overall, the mesh created had approximately 15.3 million elements for both models. Figure 2.4 shows a cross section of the mesh at the outer (pressure side and suction side) holes. Note that the light blue rectangle shown in the figure is a small gap between the showerhead hatch and blade which was not meshed.

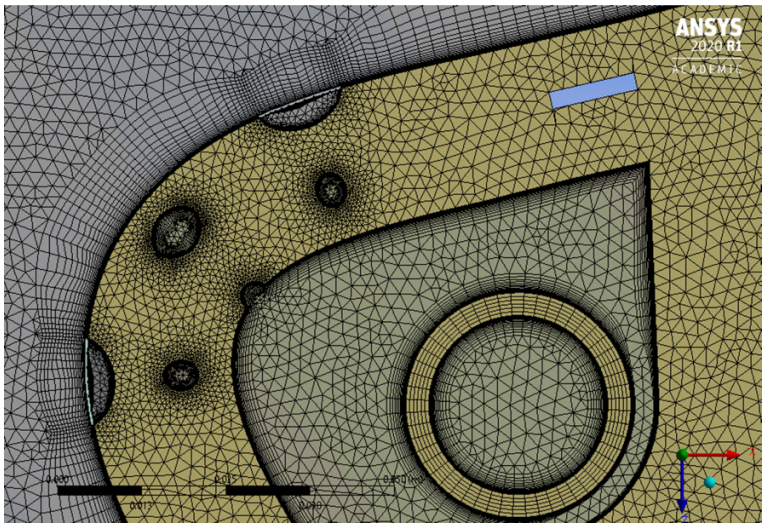

Figure 2.4: Cross Section of Fluid and Solid Meshes at Outer Holes

2.3.2 Grid Independence Test

To test the mesh, a coarse mesh, an intermediate mesh, and a fine mesh were created by varying both the size of the bulk area cells and the resolution of the inflation region. The inflation region resolution was varied by holding the thickness constant at $3D$ and changing the number of layers within the region. The coarse mesh was created with 2.3 mm bulk cells and 25 inflation layers and had 13.0 million elements. The intermediate mesh was the mesh used for simulation (described above), while the fine mesh was created with 2.0 mm bulk cells and 35 inflation layers and had 18.4 million elements. The mesh tests were performed with the impingement-fed model, for the highest blowing ratio tested $M = 3.1$. It was assumed that grid independence for this case would mean grid independence for all other cases tested.

Adiabatic effectiveness profiles were taken on a spanwise line directly downstream of the suction side hole and directly downstream of the pressure side hole on the outer surface of the blade. Adiabatic effectiveness was defined earlier by Eqn. (1.3). Because the flow fields within the holes were also key results of the study, velocity contours on midplanes through each hole were captured for each grid. Results for the suction side hole are shown in Figure 2.6, along with the adiabatic effectiveness profiles in Figure 2.5.

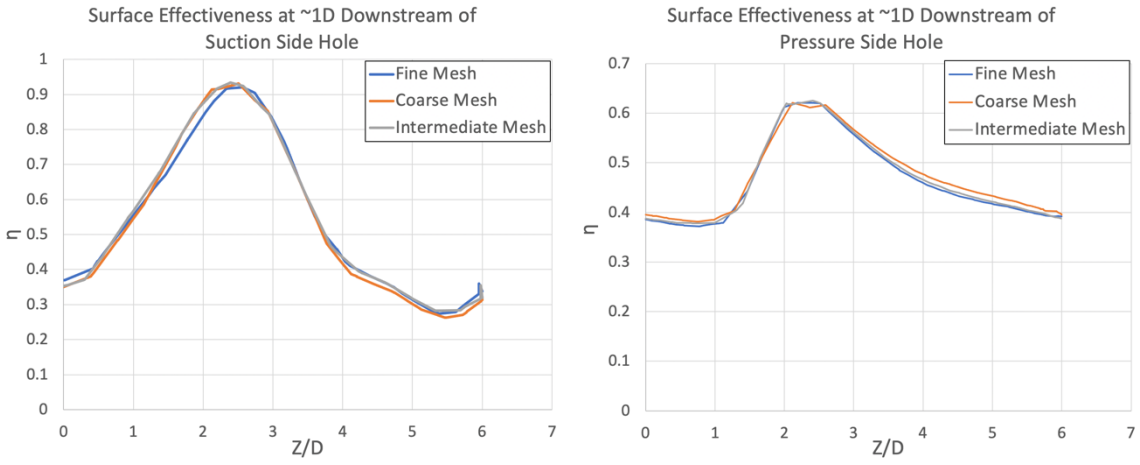

Figure 2.5: Mesh Independence Test Using Adiabatic Effectiveness at M=3.1 Impingement

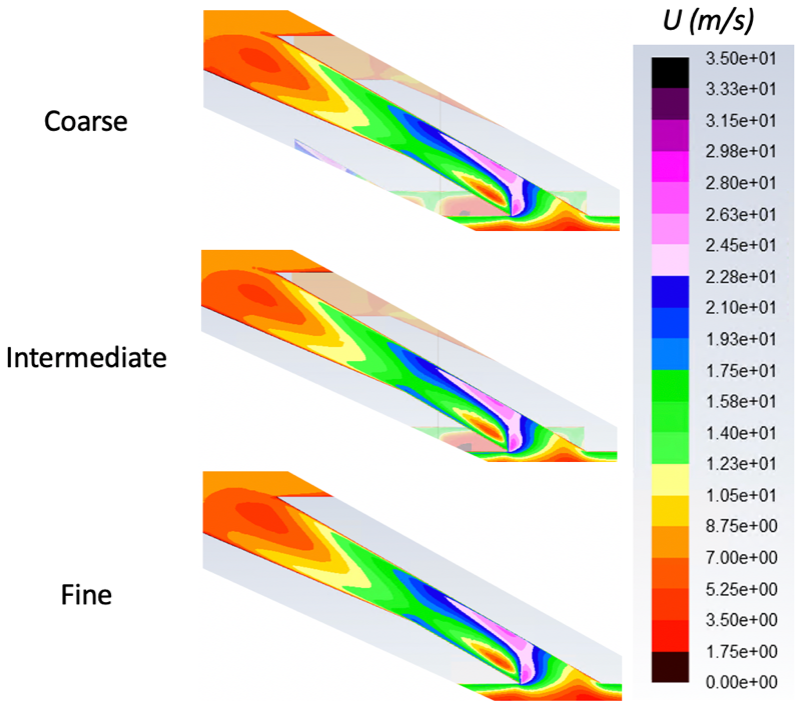

Figure 2.6: Mesh Independence Test Using Velocity at M=3.1 Impingement

The adiabatic effectiveness results show very little difference between the profiles for the different sized grids. The suction side hole shows a maximum difference of approximately 0.04 between the fine mesh and the intermediate and coarse meshes, but most areas have differences that are essentially negligible. The pressure side hole is similar, with maximum differences of approximately 0.01 between the coarse mesh and the intermediate and fine meshes. These differences were found to be negligible, especially when compared to the expected uncertainty in the computational methods used. This uncertainty caused by the mesh was also found to be similar to the experimental uncertainty calculated by Moore [5]. It should be noted that adiabatic

effectiveness contours over the entire blade surface were examined and found to be almost identical in all regions.

The velocity contour plots are almost identical, with only very slight differences visible on the fine mesh profile. Note that the contours for the stagnation and pressure side hole were also examined and found to similarly match.

Ultimately, the similarities in adiabatic effectiveness profiles and velocity contours suggest the intermediate grid is sufficiently grid independent to resolve both adiabatic effectiveness measurements and the flow fields present in the holes. Simulation with the intermediate mesh also showed that the near wall y+ values at all surfaces of the blade were less than or equal to 1 as required by the turbulence model used.

2.3.3 Inflation Region Thickness Test

As mentioned previously, the inflation regions of the mesh were created to be thick enough to encompass all boundary layers as well as the coolant jets for all holes over all blowing ratios, since these flow regions involved more complex physics, particularly in the direction away from the blade surface. Because of the high level of separation of the coolant jets in some cases, it was observed that the thickness needed to be at least between $2D$ and $3D$.

To test this more accurately and ensure the results were independent of the inflation region thickness, the thickness was varied while holding other mesh properties constant. To ensure the near wall Y+ values were still less than or equal to 1, the numbers of layers within the region were also increased as thickness was increased.

Thicknesses of $1D$, $1.5D$, $2D$ and $3D$ were tested with 22, 25, 27 and 30 layers, respectively. It was verified that all of these inflation region settings led to y+ values close to or less than 1 near the wall. Results were obtained for the impingement-fed case at $M = 3.1$, since this is the case which saw the highest level of coolant jet separation (for the pressure side hole). The same downstream adiabatic effectiveness plot from Figure 2.4 was captured for the pressure side hole, as well as the off-wall thermal field normal to the blade surface at the location of this plot. The off-wall thermal field was used to study the behavior of the separated coolant jet away from the wall. Figures 2.7 and 2.8 show these results.

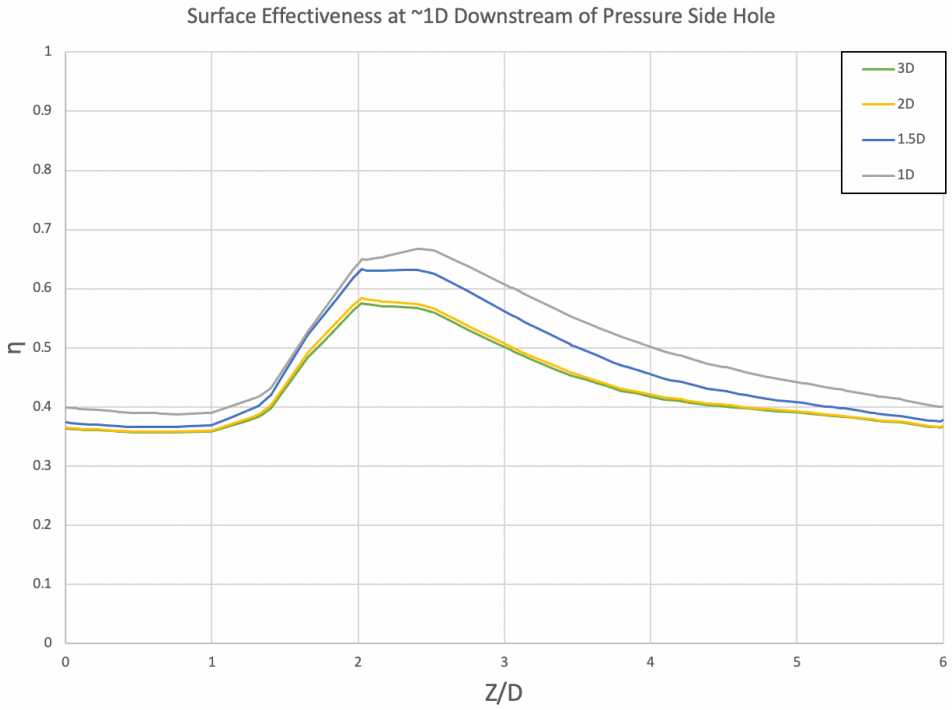

Figure 2.7: Mesh Inflation Thickness Test Using Adiabatic Effectiveness for Pressure Side Hole at $M = 3.1$ Impingement

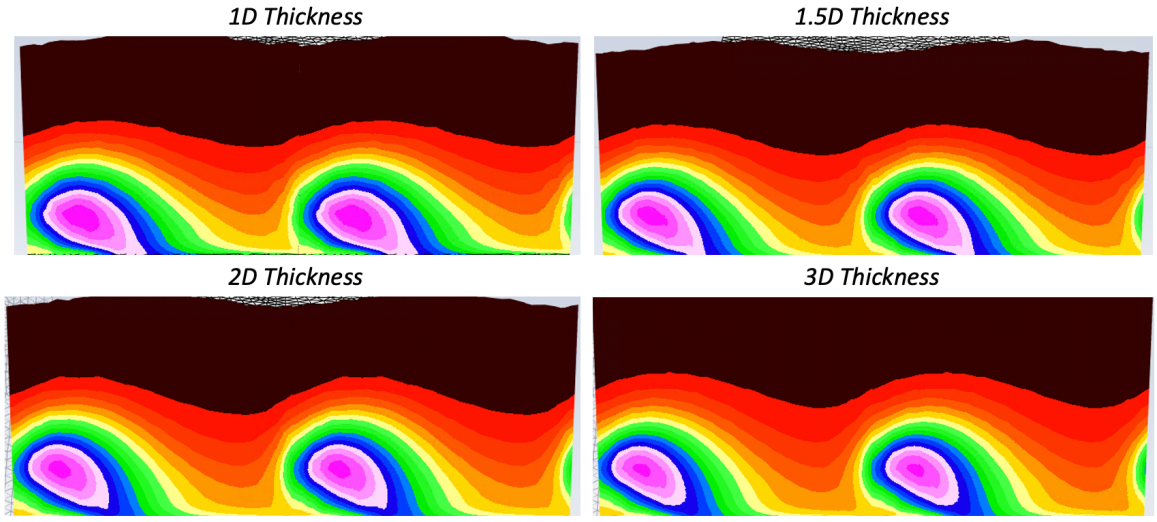

Figure 2.8: Mesh Inflation Thickness Test Using the Off-Wall Thermal Field for ~1D Downstream of Pressure Side Hole at $M = 3.1$ Impingement

The adiabatic effectiveness plots show significant differences from $1D$ to $2D$, with $3D$ being almost identical to $2D$. The thermal fields show similar results, with the jet behaving only slightly differently $1D$ to $2D$ and very similarly for $2D$ and $3D$. This is particularly evident close to the wall, with the jet being slightly better attached for the lower thicknesses and with the near-wall areas between jets behaving differently for lower thicknesses. Results for in-hole velocity contours and adiabatic effectiveness contours were also studied and found to follow the same trends. It should be noted that later results show that the higher thickness results behave more similarly to experimental results for the same case.

Because of the similarities between the $2D$ and $3D$ thickness cases, it was concluded that these thicknesses are sufficient for capturing the entirety of the coolant jet behavior, even for this extreme case of separation. Since the computational resources

required for simulating the meshes with these two inflation regions were similar, the $3D$ thickness region was used for all simulations. It was also concluded that the inflation region thickness can significantly impact the prediction of coolant jet behavior, and inflation regions which do not encompass the entire jet may poorly predict the interaction of the jet with the mainstream, possibly causing error to propagate to the near-wall areas.

2.4 SIMULATION SETUP

The CFD simulation was performed using RANS in Ansys Fluent with the RKE turbulence model and enhanced wall treatment due to the success previous studies had found using this method for leading-edge film cooling [8][9]. Fluent's baseline turbulent Prandtl number of 0.85 was employed. The blade material was set to variable thermal conductivities, such that it could be modeled as adiabatic ($k = 0.001$ W/m·K), as the material used in the experiments to measure adiabatic effectiveness ($k = 0.04$ W/m·K), and as a blade with a Biot number matching real engine conditions ($k = 1$ W/m·K) in order to study overall cooling effectiveness. The conductivity used for the experimental material was calculated in a previous study by Jones [11].

The boundary conditions were set to replicate the experimental conditions used by Moore [5], for the sake of comparison and validation. First, mainstream air was set to enter the fluid domain at 295 K, while the coolant air was set to enter the flow conditioner at 245 K. These conditions allowed matching of the density ratio to that used experimentally, where density ratio was defined by Eqn. (1.1).

To match the experimental mainstream flow field conditions, the inlet mainstream velocity was set to 7.2 m/s at a horizontal angle of 30 degrees. The mainstream turbulence was set to 5.5% with an integral length scale of 34 mm to match the turbulence measurements made in Moore's study [5]. Because the model only includes one hole-to-hole pitch in the middle of the blade, inlet conditions for the coolant were difficult to obtain, since the experimental studies only measured the inlet mass flow into the beginning of the coolant feed, and the mass flow rate into an arbitrary section of the feed in the middle of the blade could not be determined exactly. However, Moore's experiments showed that the differences between coolant flow rates through the holes at different spanwise positions along the blade were negligible, so this issue was not seen as significant. An appropriate coolant inlet mass flow rate was therefore estimated at 0.0016 kg/s, with minimal inlet turbulence to model the approximate coolant feed conditions.

The key parameter which was varied throughout the simulation was blowing ratio, M, which was changed by adjusting the total mass flow through the film cooling holes and using the total cross-sectional area of the holes to calculate the corresponding blowing ratio. The coolant was set to flow into the conditioning pipe with a constant inlet mass flow rate and out of the pipe with a varying outlet mass flow rate. The difference between the inlet and outlet flow rates was then used to achieve the correct total flow rate out of the film cooling holes. In correspondence with experimental results, blowing ratios of M=0.50, 1.16, and 3.1 were used, with $DR = 1.20$ for all cases.

The simulations were performed using a coupled pressure-velocity scheme, with a Green-Gauss node based gradient and second order upwind schemes for pressure,

density, momentum, turbulent kinetic energy, turbulent dissipation rate, and energy. Convergence was monitored both by using scaled residuals standard in Fluent, as well as point surface temperatures, film cooling hole mass flow rates, and inlet and outlet pressures versus the number of iterations. Convergence was established when the scaled residuals had dropped by at least three orders of magnitude, and when the properties of interest began to show negligible changes of less than 0.01% from iteration to iteration.

The simulations were performed using a computer with two 2.5 GHz processors and 96 GB of RAM. Convergence was generally achieved for each case in approximately 3 hours.

Chapter 3: Results[3]

This section discusses the results obtained from the CFD simulations. First, adiabatic effectiveness results and off-wall thermal fields are presented to verify the accuracy of the CFD simulation against experimental results and also to further analyze the difference in performance between the impingement and plenum fed models. Internal flow fields are then examined to explain the performance differences. Lastly, overall cooling effectiveness results are presented to study the effects of the internal flows on leading-edge internal and bore cooling as well as film cooling.

3.1 Film Cooling Results

This section discusses the isolated film cooling computational results, which are compared to experimental results to validate the CFD model. Results are also analyzed to better see the differences in film cooling performance caused by the impingement feed.

3.1.1 Experimental Conduction Effects

Adiabatic effectiveness results were obtained for both the adiabatic model case ($k = 0.001$ W/m·K) and the experimental thermal conductivity case ($k = 0.04$ W/m·K) using Eqn. (1.3) for η. Results were taken on the surface of the blade. It should be noted that a very low thermal conductivity was used for the adiabatic case instead of imposing an adiabatic wall boundary condition so that different thermal conductivities could be easily tested using the same model.

---

[3]Includes material previously published in:
Easterby, Christopher C, Moore, Jacob D and Bogard, David G. "CFD Evaluation of Internal Flow Effects on Turbine Blade Leading-Edge Film Cooling with Shaped Hole Geometries." *Proceedings of the ASME Turbo Expo*. GT2021-59780. Online, June 7–11, 2021.
The author of the current thesis was the lead author for this paper.

Because the experimental results used the low conductivity material in an attempt to isolate film effectiveness, the computational low conductivity results were first compared to the computational true adiabatic results to see if there were any conduction errors associated with the low conductivity experimental material. It was observed that the results for both conductivities were very similar, due to the fact that the experimental thermal conductivity was very small. Figure 3.1 shows this similarity for the highest blowing ratio on the impingement-fed model, with only small differences in the areas between the jets downstream and in the fact that the adiabatic effectiveness for the model properties case carries slightly further downstream on the pressure side. The holes themselves are masked for clarity of the later comparisons because the CFD results take temperatures at an imaginary surface over the outlet of the holes, while the experimental results take temperatures at the solid surface inside of the holes. It should be noted that these differences are representative of the differences seen for the other blowing ratios tested, for both feeds.

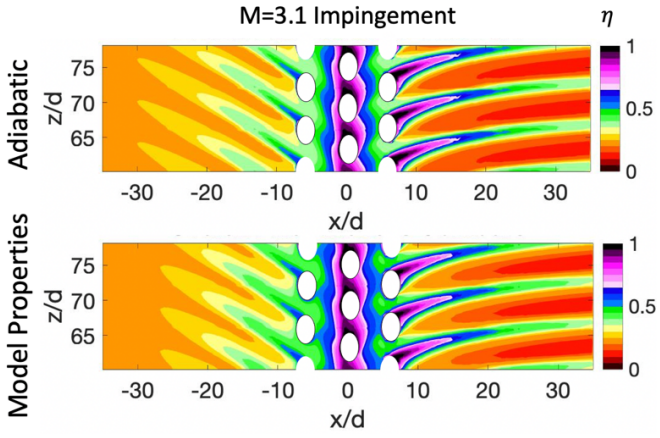

Figure 3.1: Conduction Errors in Experimental Material for M=3.1 Impingement Case

Figures 3.2 and 3.3 show the laterally averaged adiabatic effectiveness plots for the impingement and plenum cases. These figures provide a more effective comparison between the experimental adiabatic effectiveness case and the truly adiabatic effectiveness case. The adiabatic effectiveness is averaged in the spanwise direction across the blade at streamwise locations ranging from -15D (on the pressure side of the blade) to 15D (on the suction side of the blade). Again, the regions which include the holes are masked.

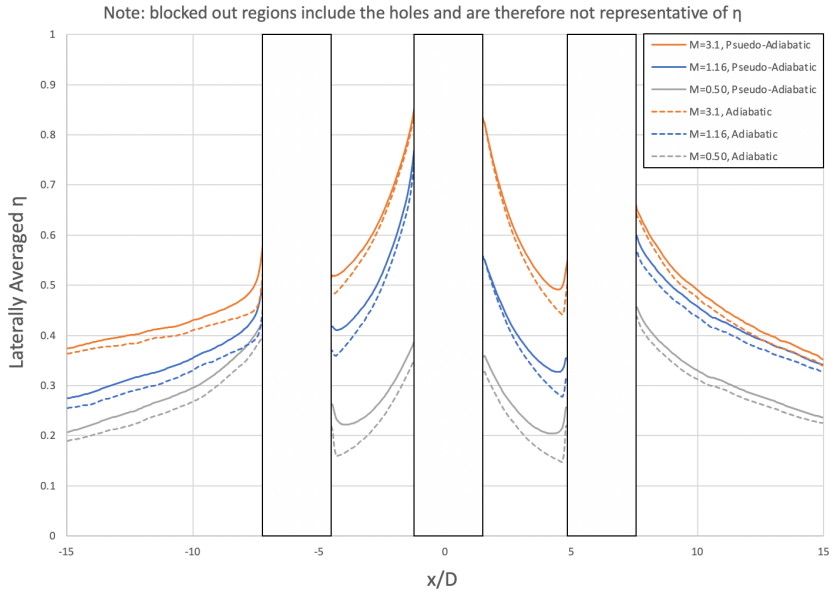

Figure 3.2: Impingement-Fed Laterally Averaged Adiabatic Effectiveness Comparisons of Pseudo-Adiabatic Material Versus True Adiabatic Material

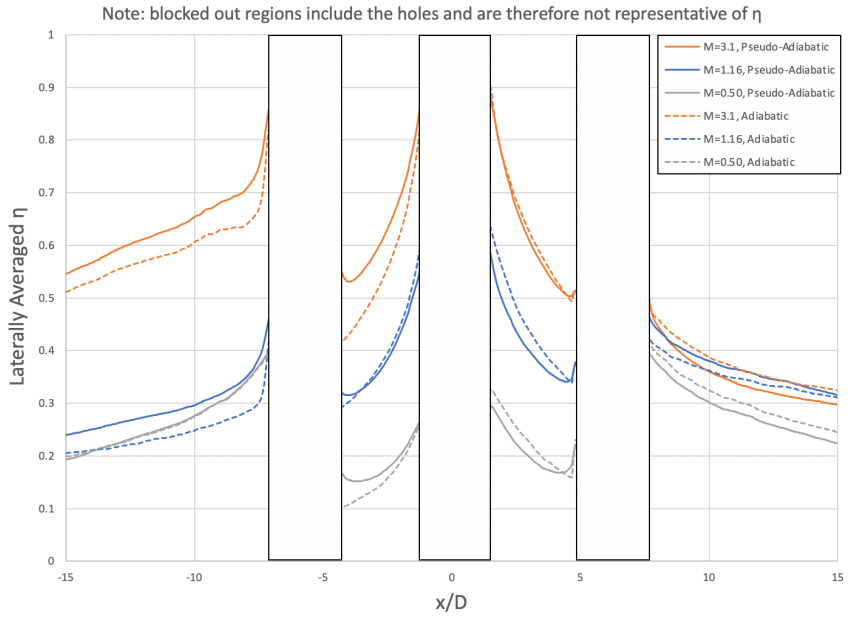

Figure 3.3: Plenum-Fed Laterally Averaged Adiabatic Effectiveness Comparisons of Pseudo-Adiabatic Material Versus True Adiabatic Material

These plots again show the small differences between the two cases, with the only significant difference being downstream of the pressure side hole for the plenum feed at $M = 3.1$ and $M = 1.16$.

Overall, this indicates that the experimental conduction errors are small, meaning the experimental results from Moore [5] accurately show isolated adiabatic effectiveness. Because this similarity was present for all adiabatic effectiveness results, further results shown in this section will only be for the experimental thermal conductivity model since comparisons will be made with experimental measurements. It should be noted that this is the first computational evaluation of the conduction errors for showerhead experiments using this low conductivity material, and the findings are important due to prior

speculation of the high potential for conduction errors caused by the small hole-to-hole spacing [5].

3.1.2 CFD and Experimental Adiabatic Effectiveness Results

Next, adiabatic effectiveness results were compared between the CFD and experimental cases to validate the CFD model. The key comparisons were between the trends caused by the different internal coolant feed geometries and the variation of blowing ratio, instead of the exact results. Figures 3.4 and 3.5 show the local adiabatic effectiveness distributions for the impingement-fed and plenum-fed models over blowing ratios $M = 0.50$, $M = 1.16$, and $M = 3.1$. These results are compared to the experimental results obtained for the same conditions by Moore [5]. Here, the pressure side of the leading edge is negative while the suction side is positive. Laterally averaged η profiles are also shown in Figure 3.6 and 3.7, comparing CFD and experimental results for the impingement and plenum feed, respectively. Lastly, Figures 3.8 and 3.9 show comparisons between the CFD impingement and plenum feed at $M = 3.1$ and $M = 0.50$, respectively.

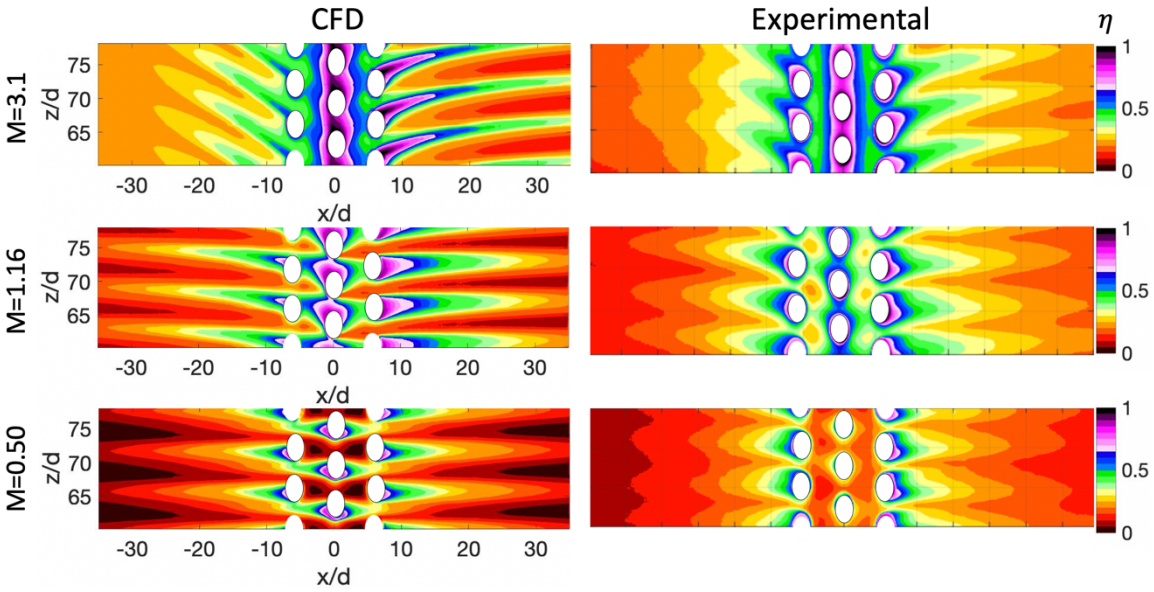

Figure 3.4: Impingement-Fed CFD Adiabatic Effectiveness Versus Experimental

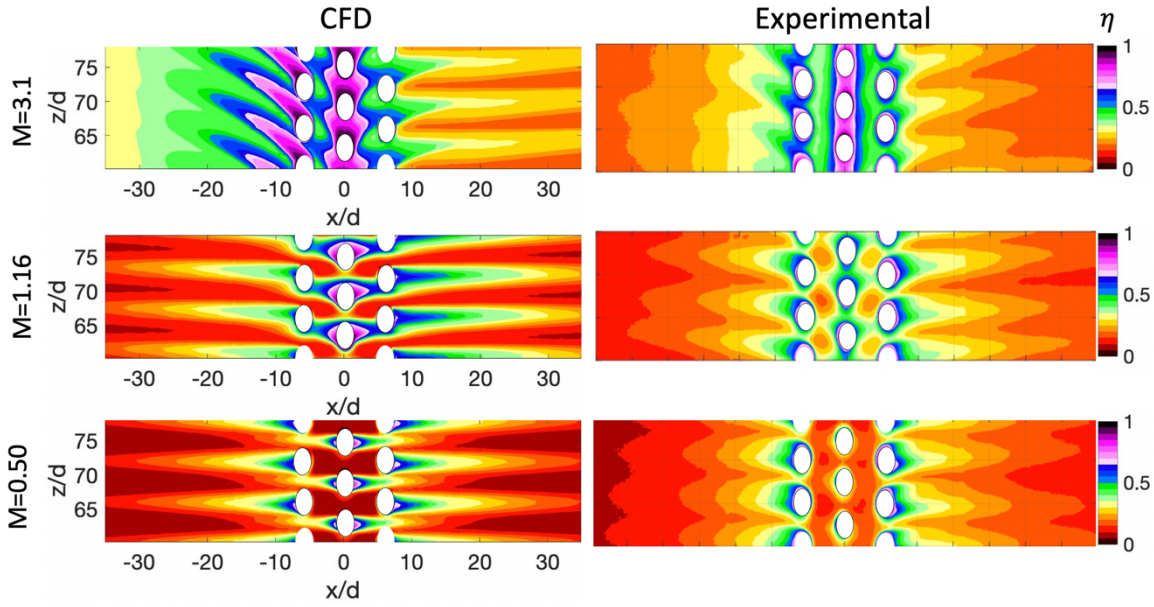

Figure 3.5: Plenum-Fed CFD Adiabatic Effectiveness Versus Experimental

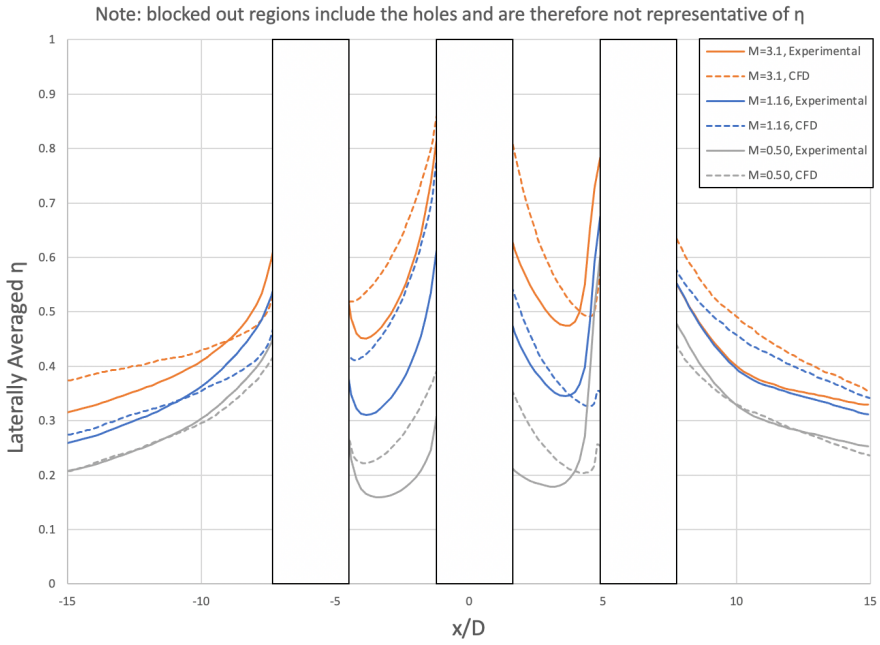

Figure 3.6: Impingement-Fed Laterally Averaged Adiabatic Effectiveness

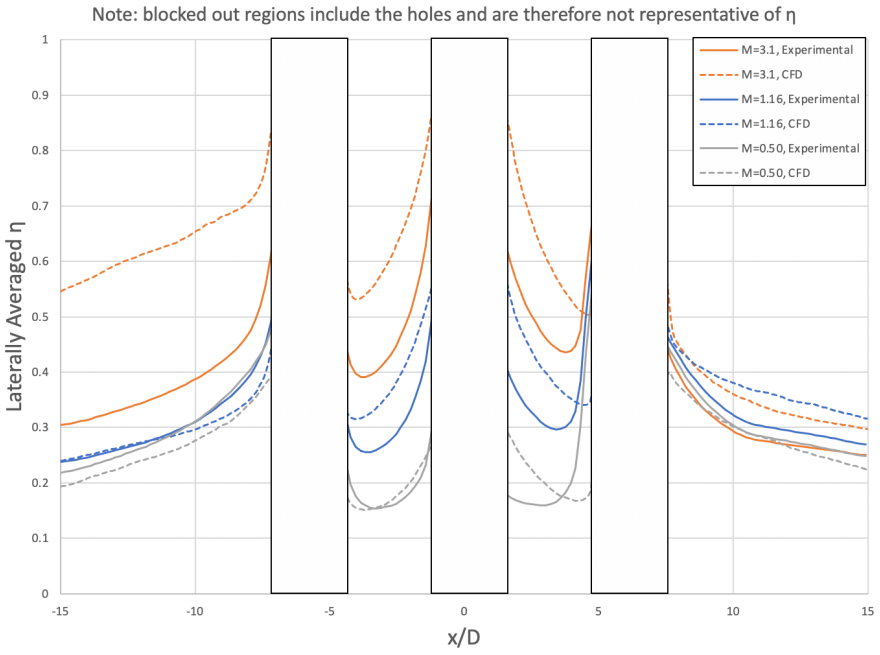

Figure 3.7: Plenum-Fed Laterally Averaged Adiabatic Effectiveness

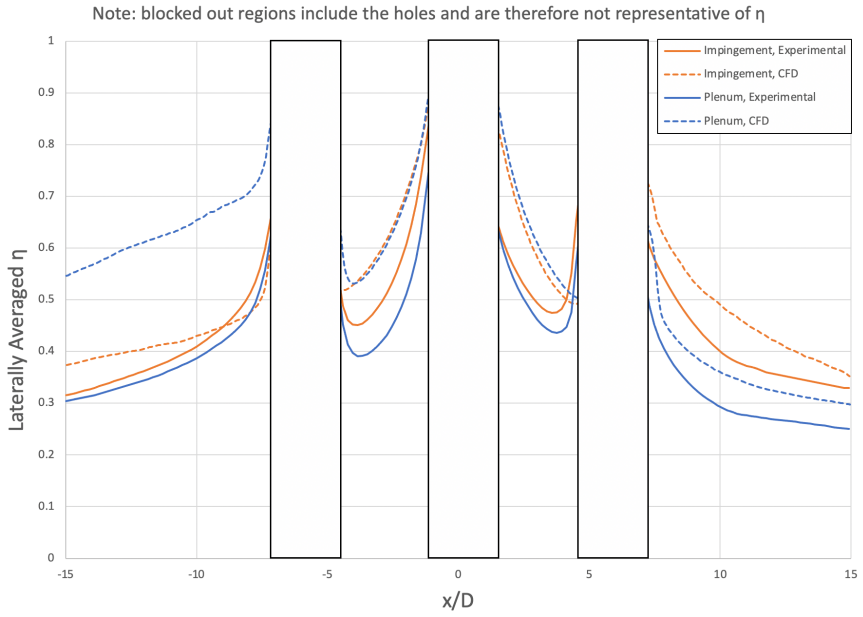

Figure 3.8: $M = 3.1$ CFD Laterally Averaged Adiabatic Effectiveness for Plenum and Impingement Feed

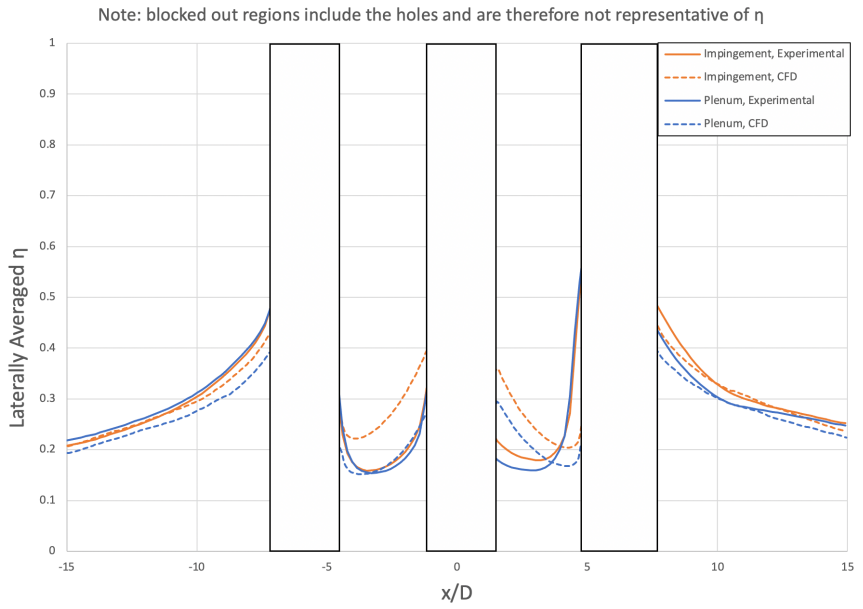

Figure 3.9: $M = 0.50$ CFD Laterally Averaged Adiabatic Effectiveness for Plenum and Impingement Feed

Overall, the CFD results show similar trends compared to the experimental results but struggle in predictions of the detailed η distributions. One key difference between computational and experimental is the fact that the CFD results show the coolant jets being carried further downstream than the experimental results. This is attributed to the fact that RANS simulation generally under-predicts fluid mixing [8][9]. The under-prediction is particularly visible at $M = 3.1$, where there are adiabatic effectiveness results of $\eta > 0.80$ at around $15D$ on the impingement case, while the experimental results do not show the coolant carrying downstream nearly as well. The under-prediction of mixing also causes the performance between the jets to be under-predicted, as most CFD results have η close to zero between jets further downstream while the experimental results show higher effectiveness between jets due to the greater turbulent dispersion of the coolant jet than predicted experimentally.

The other key difference is the CFD prediction of the pressure side hole performance at higher blowing ratios. Experimentally, Moore [5] found that the pressure side hole performed very similarly for the impingement and plenum cases, even at high blowing ratios. The CFD simulation however found a significant difference between impingement and plenum models, with the plenum model actually performing better on the pressure side hole at $M = 3.1$. The reason for this is primarily because the plenum feed leads to no separation of the coolant jet at the hole outlet, while the impingement feed leads to significant separation. This is due to the difference in the predictions of the in-hole flow fields for the two feeds, which causes the coolant to exit the pressure hole differently for either case (discussed more in the section 3.2). Why this does not match

with experimental data is somewhat unclear, but can likely be attributed both to the known RANS under-prediction of mixing, as well as a more general error predicting the flow field in this hole for the plenum case at $M = 3.1$.

Other than these differences, the CFD results do generally follow the same trends as the experimental results. As the blowing ratio decreases, the differences between plenum and impingement become less pronounced, with very similar contours between the two feeds at the lowest blowing ratio. This was the same trend observed experimentally. However, Figure 3.9 shows that there are somewhat significant differences (approximately 0.07) between the plenum feed and impingement feed in the area between the stagnation row of holes and the pressure side row of holes at $M = 3.1$. The reason for this may be internal cooling caused by the impingement feed, discussed further in section 3.3.

The experimental results also found the most significant differences in performance to be at the higher blowing ratios downstream of the suction side hole, with the impingement fed model performing much better, a trend that is shown very well by the CFD results. It should be noted that the cause of this trend was one of the primary reasons for this study, so it was encouraging to see this trend predicted computationally.

While the plenum-fed pressure side CFD results do not match well at the highest blowing ratio, they show the correct trends for $M = 1.16$ and $M = 0.50$, performing very similarly to the impingement-fed model. Lastly, the stagnation row performs generally as expected, with both feed models performing similarly for all blowing ratios, although

some error is again caused by the under-prediction of coolant mixing with the mainstream.

3.1.3 CFD and Experimental Off-Wall Thermal Fields

Next, thermal fields of θ were obtained using the following contour planes: spanwise and perpendicular to the blade's surface directly downstream of the suction and pressure side holes, spanwise and perpendicular to the blade's surface through the middle of the stagnation hole, and streamwise and perpendicular to the blade's surface through the middle of the outer holes. Figure 3.10 shows the thermal fields downstream of the suction side hole. CFD results are compared to experimental results from Moore [5] only for the impingement case, since experimental results were not available for the plenum case.

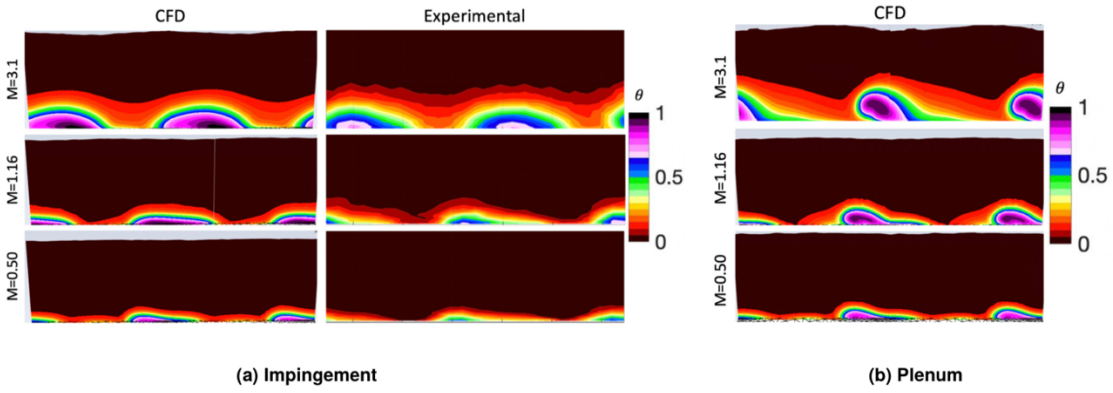

Figure 3.10: Off-Wall Thermal Fields Downstream of Suction Side Hole

The impingement-fed case results match well with those obtained experimentally, showing that the coolant jet remains well attached even at $M = 3.1$. The plenum case

results explain why the performance downstream of the suction hole is so much better for the impingement case, as the plenum fed model has detachment at the highest blowing ratio.

Figure 3.11 shows the results downstream of the pressure side hole for the same cases. These thermal fields show the reason for the poorer pressure side performance of the impingement-fed case, as there is significant separation at $M = 3.1$ and even some separation at $M = 1.16$. These results show some agreement with the experimental results, though the CFD results again show generally cooler temperatures due to the under-predicted mixing. For impingement, the CFD simulation also predicts the jets to be further from the wall for M=3.1 than the experimental results show, and predicts slight separation for M=1.16, disagreeing with the experimental results. However, the CFD results match well with the experiments on the outer edges of the coolant and between the jets.

The plenum-fed model shows only slight separation at $M = 1.16$ and, surprisingly, no separation at $M = 3.1$, explaining the better performance seen on the pressure side. This trend is unexpected and is speculated to be due to strong jet-to-jet interactions which block off the mainstream gases between jets. As mentioned previously, this greater performance does differ from experimental results, due to a likely error in predicting the pressure side hole flow field. Note that some figures show areas in

which θ is slightly below zero, causing the color map to be cut off.

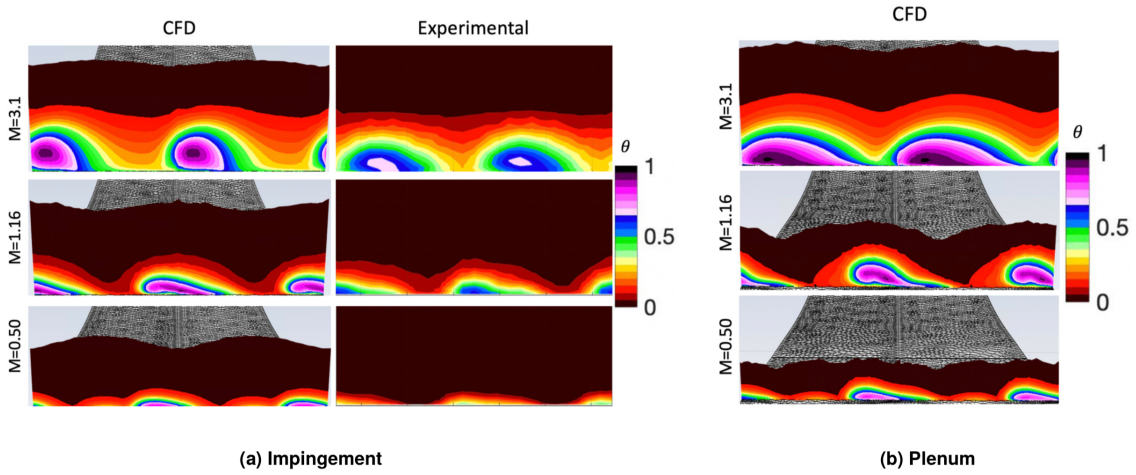

Figure 3.11: Off-Wall Thermal Fields Downstream of Pressure Side Hole

Next, Figure 3.12 shows the θ contours through the center of the stagnation row of holes. Here, only the plenum results are compared to experimental results from Moore [5], as these were the only results from this contour available experimentally. Again, the thermal fields match well with those obtained experimentally, with the coolant carrying between holes only slightly better for the CFD case. The θ values within the hole also match well with the experimental results, as does the propagation of coolant away from the wall. Comparing impingement to plenum, the impingement case has slightly better performance between holes for $M = 3.1$ and $M = 1.16$, and both feed configurations have essentially no adiabatic effectiveness between holes for $M = 0.50$. It should also be noted that the $M = 0.50$ case correctly predicts the ingestion of mainstream gases into the hole, although the ingestion is greater for the experimental measurements.

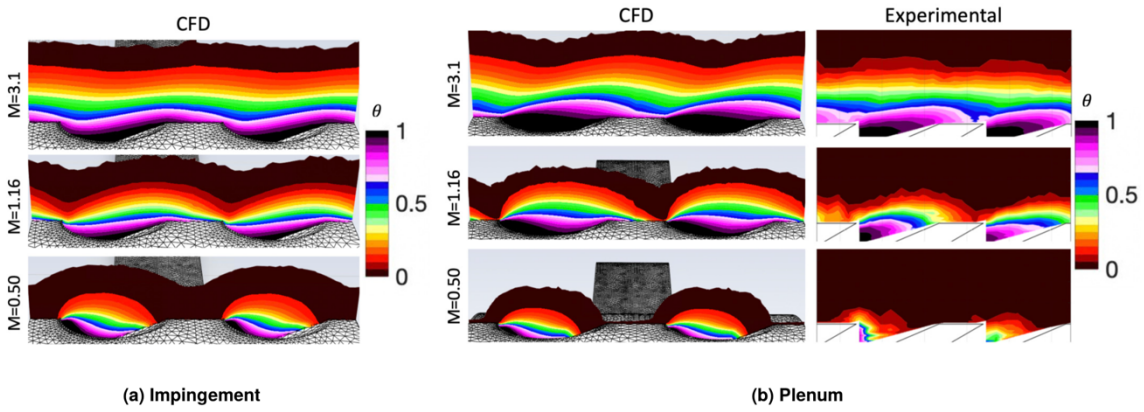

Figure 3.12: Off-Wall Thermal Fields Downstream of Stagnation Row Hole

Lastly, Figure 3.13 shows a streamwise plane thermal field through the middle of the outer holes. For these, only the impingement results are compared to experimental results from Moore [5]. The CFD results again match with the experimental, although the CFD results show a wider stagnation row jet between the holes. This result is slightly unexpected, as the underpredicted mixing should have caused a narrower jet. This suggests that the area near the wall for the stagnation row jet is another area in which the CFD is not accurately predicting the behavior of the coolant jet, though here the differences are small. The impingement case and plenum case perform very similarly between holes for $M = 3.1$ and $M = 1.16$, with negligible cooling between holes for both feeds at $M = 0.50$. These figures also show another view of the $M = 3.1$ separation occurring on the suction side for the plenum case, the $M = 3.1$ attachment on the suction side for the impingement case, and the $M = 3.1$ separation on the pressure side for both cases.

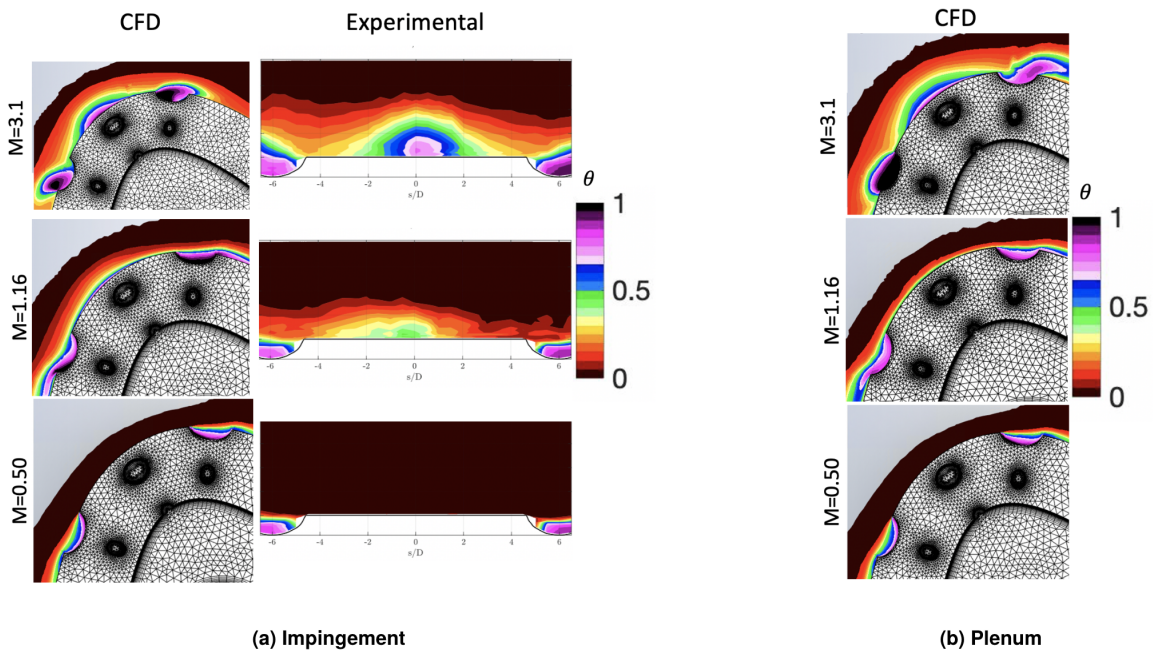

Figure 3.13: Off-Wall Thermal Fields on Midplane through Outer Holes

Overall, these adiabatic effectiveness and thermal field results show several important points. First, the CFD simulation was able to successfully predict many important aspects of the film cooling, particularly the separation or attachment of coolant jets at the outlets of the holes. It also effectively captured almost all of the major trends relating performance to blowing ratio. The main downsides of the CFD results compared to experimental results was its sometimes-significant under-prediction of coolant mixing with the mainstream air, and its error in predicting the pressure side hole flow field for the plenum case at $M = 3.1$. However, it was verified that the RANS simulation is able to model most of the important aspects of the flow fields, leading to the conclusion that it can be used to gain insight into the internal flow fields involved in leading-edge

showerhead film cooling. Additionally, the thermal fields effectively show why the plenum and impingement cases perform differently in terms of film cooling, due to the attachment and separation caused at the hole outlets by the feeds.

3.2 INTERNAL FLOW RESULTS

The internal flow fields obtained computationally that caused the differences in effectiveness are presented in this section. First, velocity vector fields are presented to illustrate the general flow field in the internal coolant chamber. Velocity contours inside the holes are then shown to see what the flow field looks like inside the holes themselves, in an effort to explain the differences in cooling performance between the two internal feeds. Lastly, discharge coefficients are presented to study how the internal feeds affect the mass flow through the holes.

3.2.1 Velocity Vector Fields

Figures 3.14 and 3.15 show the velocity vector fields for the $M = 3.1$ case for both feed models.

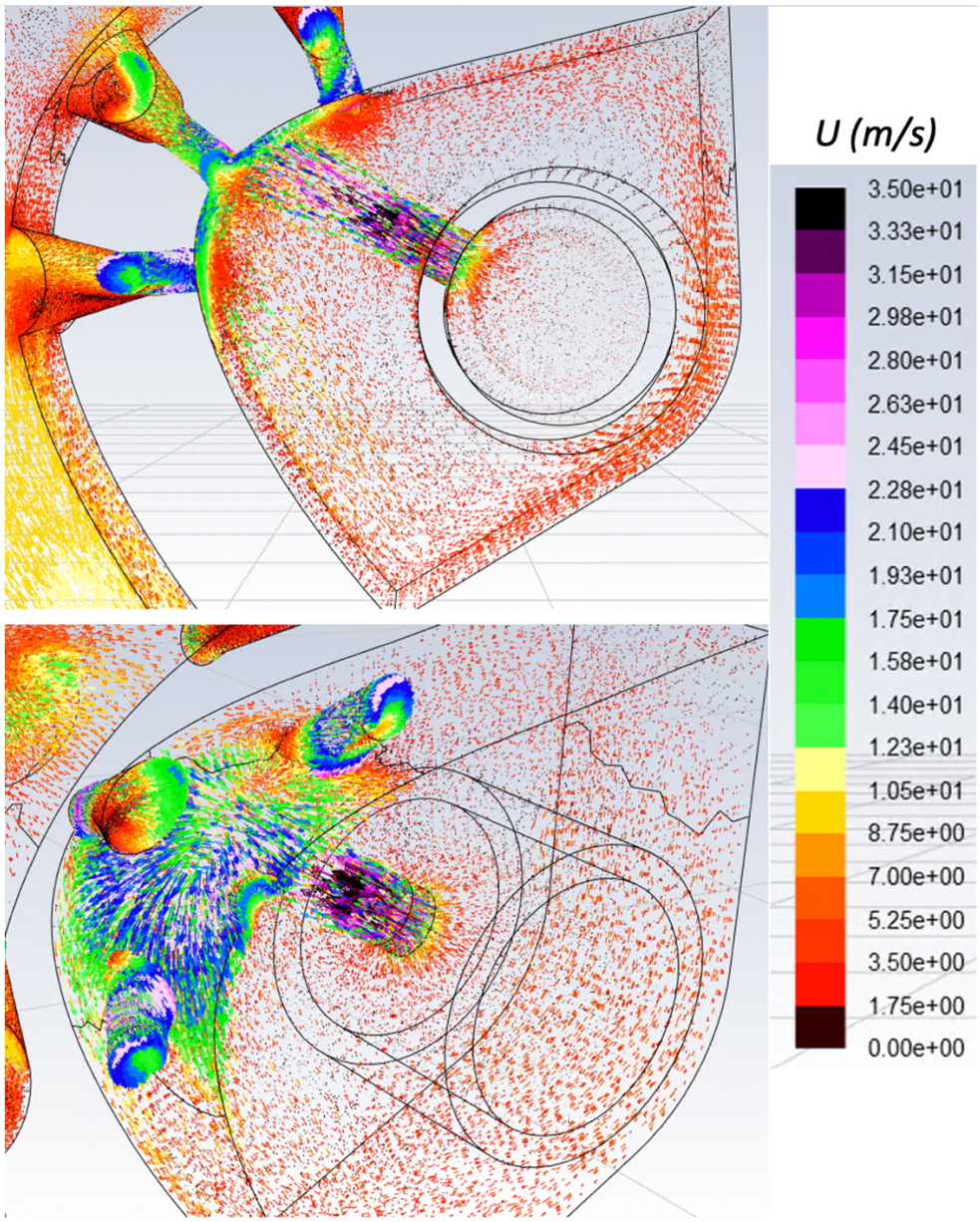

Figure 3.14: Velocity Vector Field for Impingement Feed at $M = 3.1$

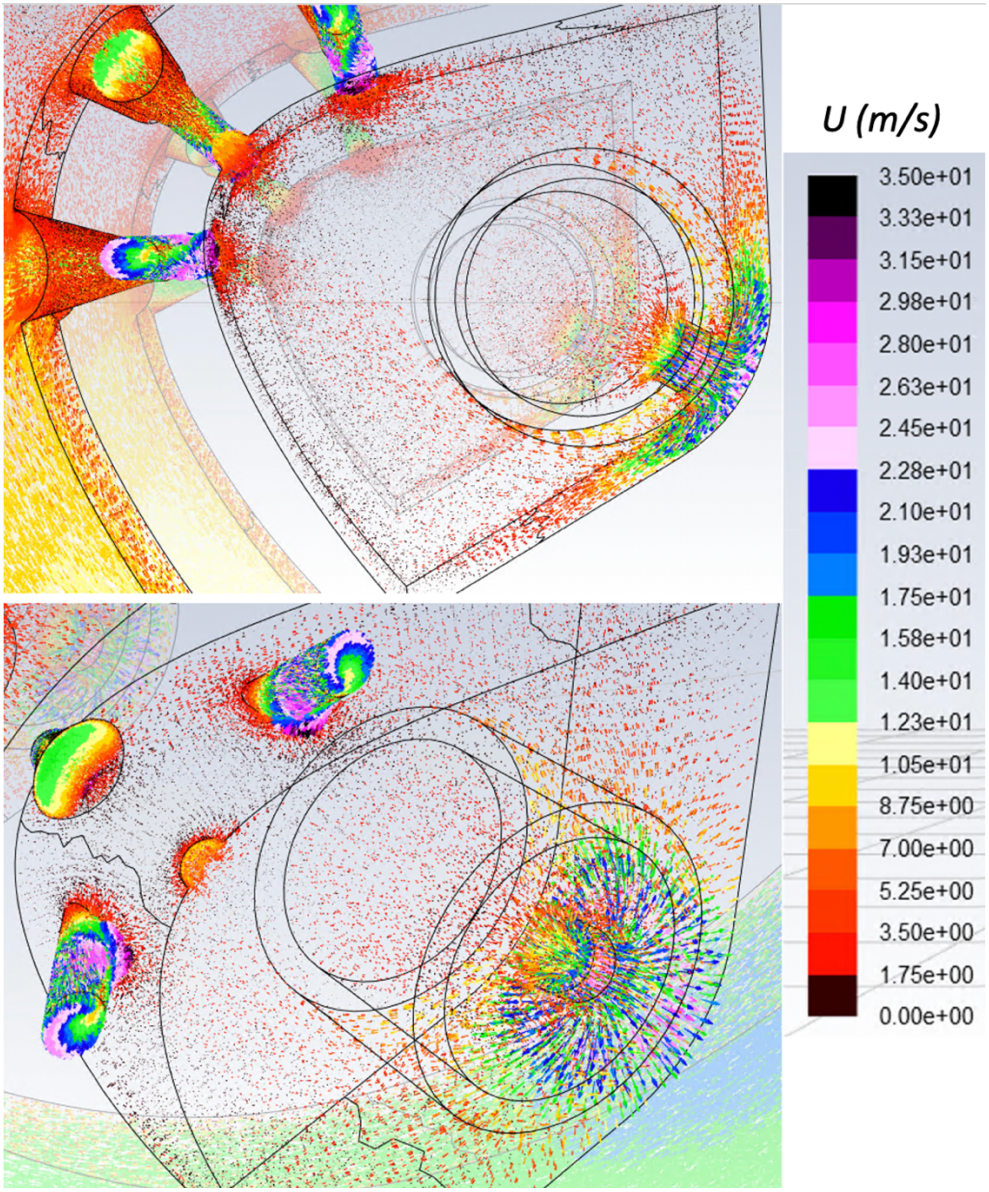

Figure 3.15: Velocity Vector Field for Plenum Feed at $M = 3.1$

The vector fields provide a good visualization of how the coolant enters the holes for both cases. The pseudo-plenum model is shown to effectively model a plenum feed, as the velocities in the internal chamber near the holes are essentially negligible relative

to the velocities present in the holes and mainstream, and the coolant enters the holes in a generally uniform way even at the highest blowing ratio tested.

The impingement feed is shown to have significantly different internal flow conditions, as expected. Because of the angle of the wall at which the jet impinges, most of the coolant goes towards the suction side hole and stagnation row hole. Because of this flow, the coolant enters these two holes at an angle which causes rotation within the film cooling holes themselves. This rotation will be further analyzed using the velocity contours. The pressure side hole actually receives some coolant directly from the impingement jet and some coolant which travels all the way around the feed pipe to the pressure side inlet, leading to a feed from the co-flow direction as well as from the counter-flow direction. This complex feed for the pressure side hole affects the flow through the hole and partially explains its poorer performance, as well as the fact that it performs similarly to the plenum case pressure side hole.

3.2.2 In-Hole Velocity Contours

The velocity contours in the holes show the effects of these inlet conditions. Contours were taken on a midplane through the holes and on four planes perpendicular to the flow in the holes. Velocity vector fields were also obtained on these four perpendicular contour planes for all three holes in order to see the rotation.

Figure 3.16 shows the relation between blowing ratio and internal velocity for the suction side hole midplane contour for both feed cases. For $M = 3.1$, the differences between the impingement feed and plenum feed are very significant, consistent with the

differences in adiabatic effectiveness between the feeds for this case. At the lower blowing ratios, the temperature results show that the impingement case behaves similarly to the plenum and thus has smaller internal flow field effects. This trend was also seen for the stagnation row hole and pressure side hole, but the suction hole showed the greatest differences at $M = 3.1$.

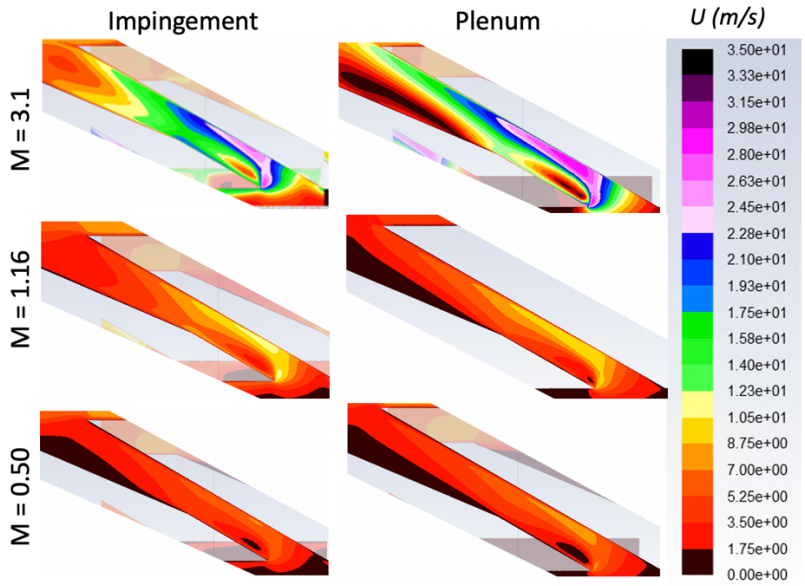

Figure 3.16: Velocity Midplane Contours in Suction Side Hole Versus Blowing Ratio

While contours were recorded at all simulated blowing ratios, because the primary performance differences were observed at the highest blowing ratio, Figures 3.17 through 3.20 are shown only for the $M = 3.1$ case. Figure 3.17 shows the midplane velocity contours for all three holes at $M = 3.1$, while Figures 3.18 through 3.20 show the perpendicular velocity contours for the three holes at $M = 3.1$.

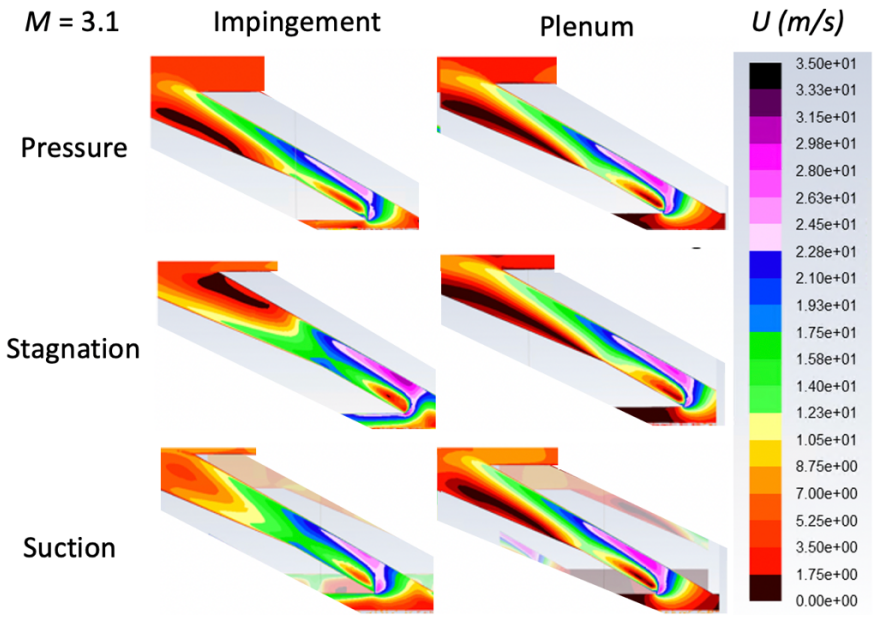

Figure 3.17: Velocity Midplane Contours at $M = 3.1$

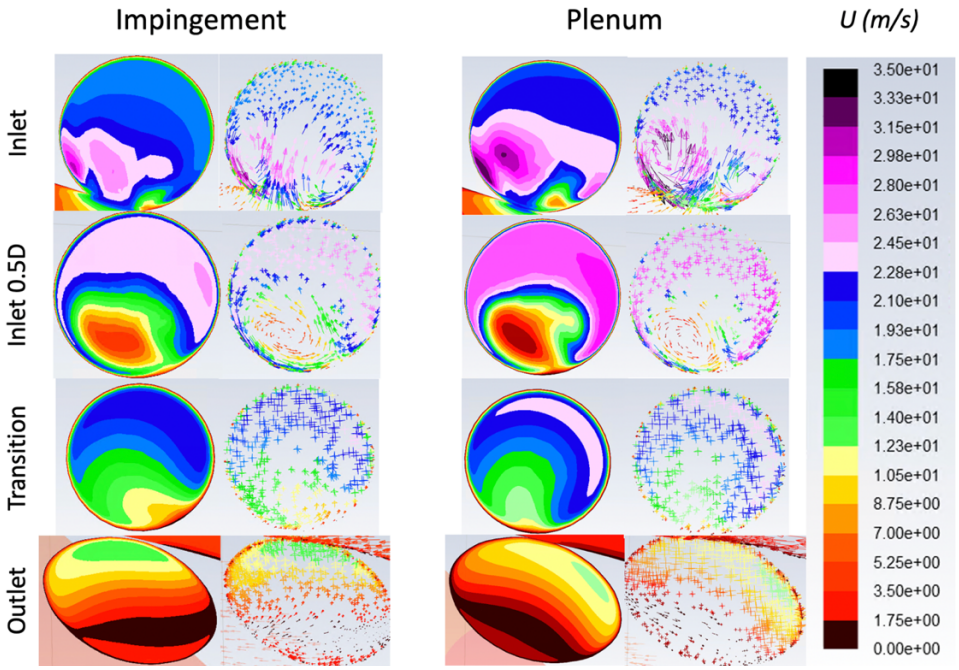

Figure 3.18: Velocity Perpendicular Contours for Pressure Side Hole at $M = 3.1$

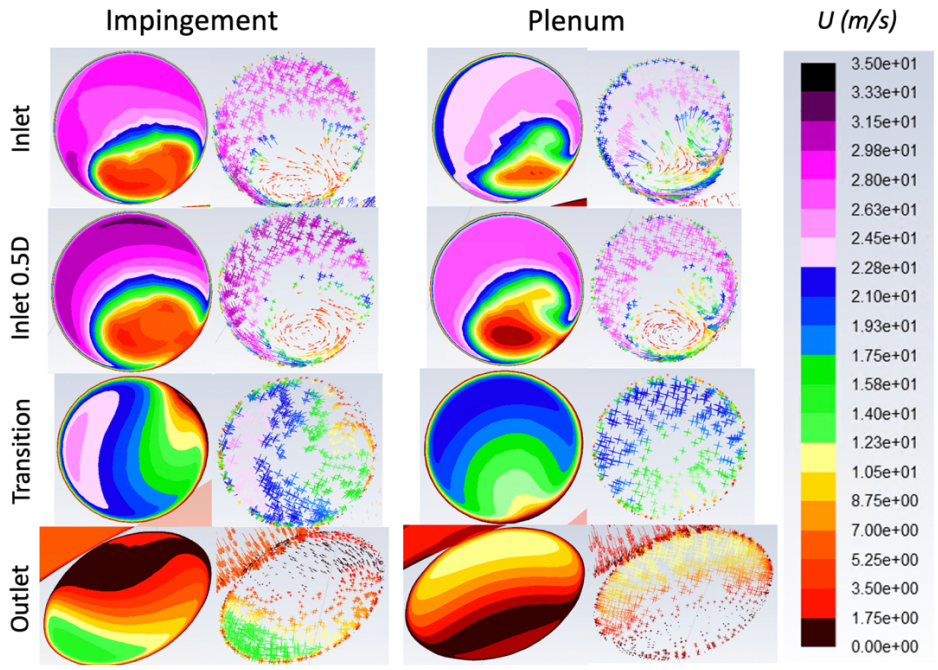

Figure 3.19: Velocity Perpendicular Contours for Stagnation Row Hole at $M = 3.1$

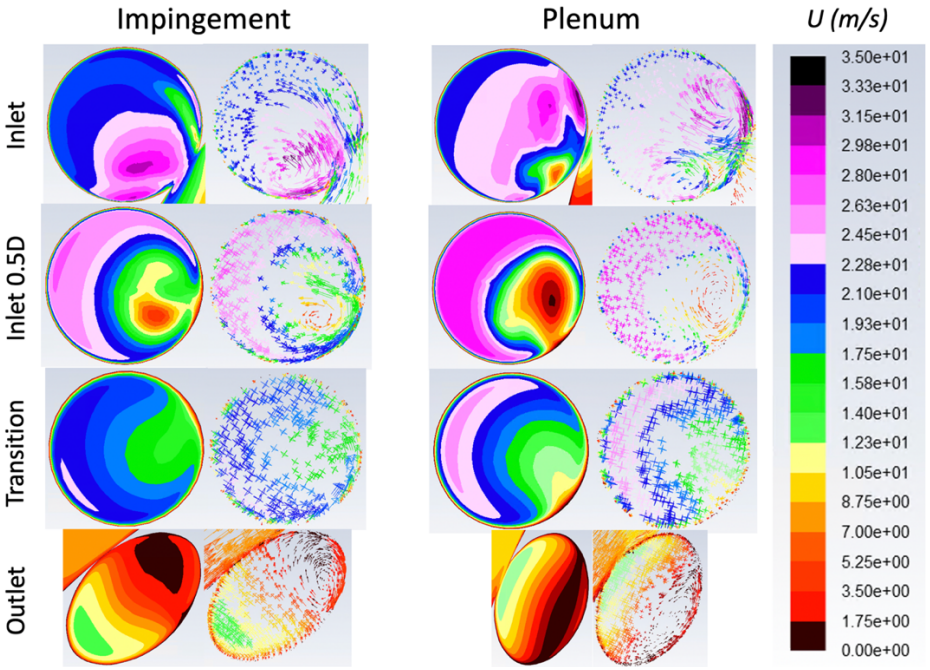

Figure 3.20: Velocity Perpendicular Contours for Suction Side Hole at $M = 3.1$

Using these contours together shows why the impingement feed and plenum feed perform similarly in some areas and differently in others. The pressure side hole midplane contours look very similar for both feed configurations, with the main coolant jet, represented by the highest velocity areas, staying near the top of the hole throughout, with separation on the bottom of the hole outlet. However, the perpendicular contours in Figure 3.18 show that the impingement-fed jet does rotate slightly compared to the plenum case. Additionally, the velocity gradient across the outlet of the hole in Figure 3.18 is slightly less steep for the plenum case, suggesting that the plenum feed has better spreading of the coolant jet in the expansion section while the impingement feed leads to a coolant jet more skewed to the top of the hole. The greater spreading for the plenum case leads to the better performance seen in the adiabatic effectiveness results (Figures 3.4 and 3.5). This difference causes the pressure side impingement hole to perform more poorly than the plenum case at $M = 3.1$. For the impingement case, the fact that the jet exits near the top of the hole and experiences separation on the bottom causes poor attachment downstream, as the coolant jet must be turned to the surface by the mainstream air more for attachment to occur. This is validated from the thermal fields showing some separation downstream of the pressure hole for this case at $M = 3.1$. The plenum case also exits near the top, but the better spreading of the coolant jet leads to the attachment seen in Figure 3.11.

Looking at contours for the stagnation hole in Figure 3.19, it is clear significant rotation is occurring in the impingement case as a result of the flow field created at the inlet. The contours show the jet is rotated more than 90 degrees at the outlet (compared to

the plenum case) and the impingement case also experiences higher velocities due to the higher velocity coolant entering the hole. For the impingement feed, this means the jet exits near the pressure side of the hole, while for the plenum case it exits near the top of the hole. As with the pressure hole, the jet exiting on the top means it is less likely to remain attached downstream for the plenum case, although the thermal fields show that the greater pressure at the stagnation point is enough to turn the plenum jet such that is does remain attached even at $M = 3.1$. Still, the impingement case exiting away from the top means it stays attached better downstream, a fact supported by the adiabatic effectiveness contours (Figures 3.4 and 3.5) showing slightly better performance on the stagnation row for the impingement case.

Velocity contours for the suction hole shown in Figure 3.20 also show significant jet rotation within the hole. In this case, the jet rotates from the top of the hole to the upstream side of the hole, again promoting better downstream attachment when compared to the plenum case which has the jet exiting on the top. This explains the significantly higher suction side performance of the impingement case compared to the plenum case.

Overall, it is concluded that the rotation caused by the impingement jet in leading-edge showerhead regions can significantly impact the film cooling performance of shaped holes. Rotation (or lack of rotation) that caused the high velocity regions of coolant to exit on the top of the hole universally led to poor attachment downstream, while rotation which caused the jet to exit anywhere else encouraged better attachment.

3.2.3 Discharge Coefficients

Lastly discharge coefficients were analyzed to see the effect of the internal feeds on the mass flow through the holes. Discharge coefficients were calculated using the incompressible form of the equation (due to experimental data showing the incompressible and compressible results were very similar) listed below.

$$C_d = \frac{\dot{m}}{A_h\sqrt{2\rho_c(P_{t,c}-P_{\infty,local})}} \tag{3.1}$$

Here, $\dot{m}$ is the mass flow rate through the holes, A_h is the hole metering area, ρ_c is the coolant density, $P_{t,c}$ is the total pressure of the coolant in the internal chamber and $P_{\infty,local}$ is the external static pressure at the hole outlets. Discharge coefficient here is essentially the actual mass flow rate over the theoretical (inviscid) mass flow rate based on the pressure difference between the inlet and outlet of the hole. However, it should be noted that this definition does not take into account the effects of the expansion section of the hole on the theoretical mass flow rate, meaning it is possible to have C_d values greater than 1.0.

To compare computational discharge coefficients with experimental data, results were taken for all three rows of holes, giving a showerhead discharge coefficient ($C_{d_{sh}}$). This was calculated using the total mass flow rate through all three rows, the total metering area of all three rows, a coolant pressure measured on the back wall of the coolant chamber (in the same area as the experimental pressure tap), and the average of the static pressures at the outlets of all three holes. The CFD results are shown below in

Figure 3.21a compared to experimental results from Moore [5] in Figure 3.21b. Values are plotted against pressure ratio (PR), defined below.

$$PR = \frac{P_{t,c}}{P_{\infty,local}} \tag{3.2}$$

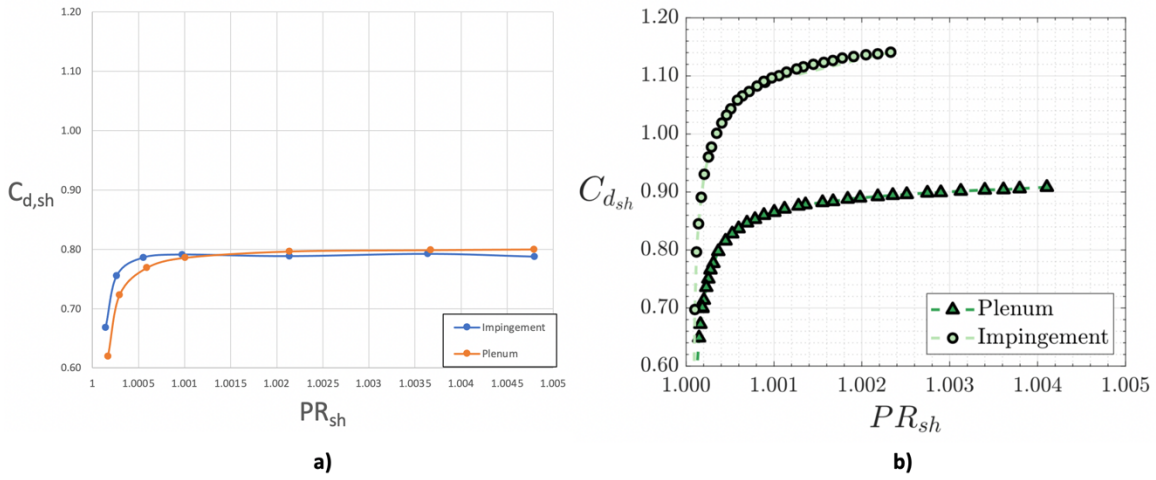

Figure 3.21: Computational and Experimental Discharge Coefficients Versus Pressure Ratio

The experimental data shows significant differences between the impingement and plenum case, with the impingement-fed model having significantly higher discharge coefficients (over 1.10 at the highest pressure ratio) than the plenum case (around 0.90 for the highest pressure ratios). Both the CFD and experimental data do show sharp declines towards zero at lower pressure ratios, but the CFD case looks very different compared to experimental data, with both the plenum and impingement models plateauing at approximately 0.80.

The reason for this discrepancy is not obvious but could be due to an inherit flaw in the RANS model's prediction of the pressures involved in calculating discharge coefficients. If true, this would further explain some of the differences between the CFD and experimental results discussed earlier. The fact that the computational discharge coefficients were smaller than the experimental measurements indicates that the pressure recovery in the expansion section of the hole was underpredicted by the simulations. This suggests that the in-hole separation regions predicted computationally were larger than they were experimentally, possibly because of the computational holes not matching perfectly with the built holes. This difference would likely be most significant at the sharp corners and hole inlets.

Another important conclusion of this study was the relative insensitivity of the measurements made by the internal pressure tap to its location in the coolant chamber. As expected, the plenum feed was found to have very similar pressures in almost all locations of the chamber, but the impingement feed was also found to have similar pressure values throughout the chamber. The exception was areas near the impingement location of the coolant jet, meaning the internal surface of the leading edge for the impingement feed and the middle of the back chamber wall for the plenum feed. For these areas, the pressure was affected significantly by the coolant impingement, as expected.

3.3 Overall Cooling Effectiveness Results

This section covers the computational study of the effects of the internal feed on overall cooling of the leading edge. This includes film cooling as well as internal and bore

convective cooling, so a thermal conductivity of $k = 1$ W/m·K was used to approximately match the Biot number present in real engine conditions. This value was chosen according to previous studies by Mouzon et al. and Ravelli et al. [6][7]. Results are first shown for overall cooling effectiveness, with comparisons to adiabatic effectiveness results to visualize the internal and bore convective cooling effects. Heat flux and heat transfer coefficient results on the internal surfaces of the blade are then presented to help explain the differences in convective cooling.

3.3.1 Overall Effectiveness Results

Here, overall effectiveness results are shown for both feeds with comparisons to adiabatic effectiveness results from earlier. The overall effectiveness is calculated in essentially the same way as adiabatic effectiveness, but by using surface temperatures for a conducting blade. Equation 3.3 shows this below.

$$\phi = \frac{T_\infty - T_m}{T_\infty - T_{c,i}} \tag{3.3}$$

Here, T_m is the surface temperature of the conducting blade and $T_{c,i}$ is the initial temperature of the coolant before any internal heating has occurred. For correct results, the Biot number and the ratio of external to internal heat transfer coefficients must be matched to engine conditions. The former was accomplished using the thermal conductivity mentioned above while the latter was accomplished by matching Reynolds numbers.

Figure 3.22 shows the overall effectiveness contours for the impingement and plenum feed, while Figure 3.23 shows the same results for adiabatic effectiveness.

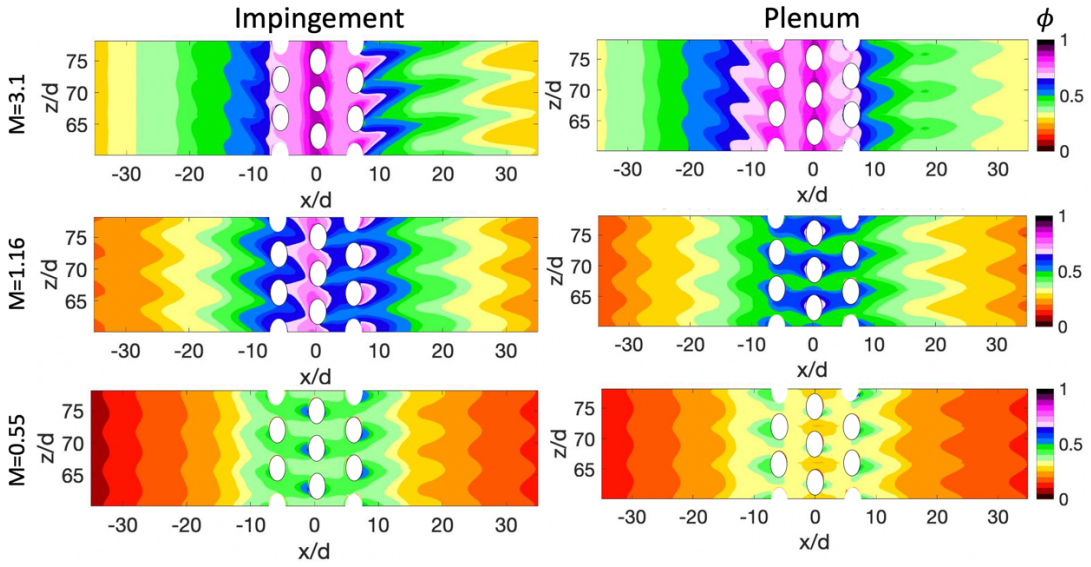

Figure 3.22: Overall Effectiveness for Impingement and Plenum Feed

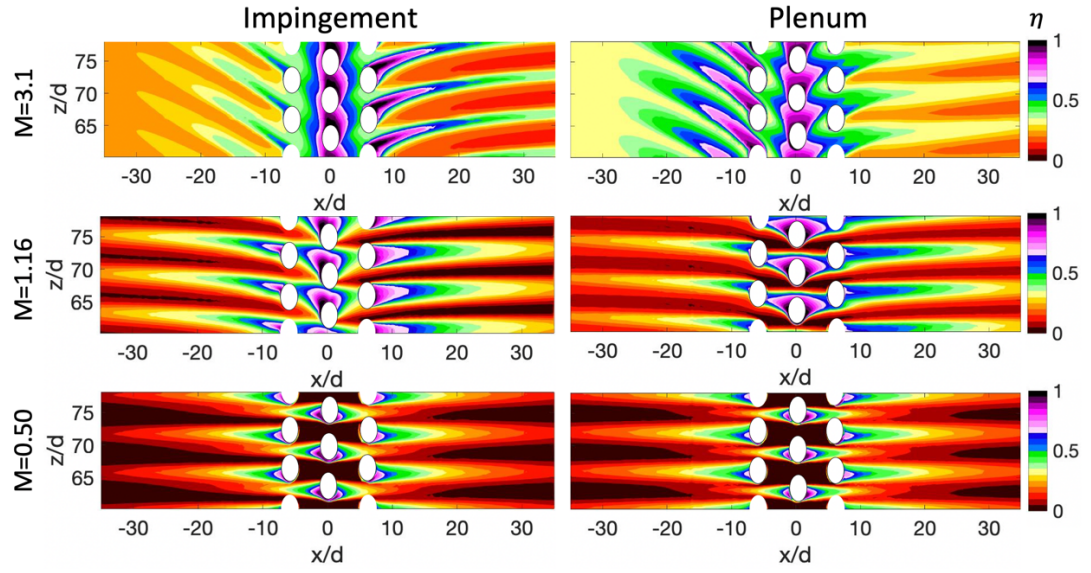

Figure 3.23: Adiabatic Effectiveness for Impingement and Plenum Feed

As the figures show, there are significant differences between the overall cooling performance of the impingement and plenum feed. However, it is important to note where these differences come from the film cooling differences and where they come from internal or bore cooling differences. This can primarily be seen by comparison with the adiabatic effectiveness data. For example, at $M = 3.1$ the impingement feed performs better than the plenum feed on the suction side while the opposite is true for the pressure side. Looking at the adiabatic effectiveness plots shows this is primarily due to the difference in film cooling between the feeds on these sides, and it is difficult to see any differences caused by internal or bore cooling.

Looking at the lower blowing ratios better reveals the internal and bore convective cooling differences, since the adiabatic effectiveness contours are more similar. At $M = 1.16$ and $M = 0.50$, the impingement feed has noticeably higher ϕ values in the showerhead region of the blade, despite the film cooling performance being similar in this area. This suggests the impingement feed is causing better internal or bore cooling in this area, which may be expected due to the coolant jet impinging on the back of the leading-edge surface. It should be noted however that the studies by Mouzon et al. and Ravelli et al. discussed earlier found an impingement feed to have negligible effects on overall cooling of a leading-edge showerhead at $M = 2$ and $M = 1$ due to the in-hole bore cooling dominating over any internal cooling [6][7]. This difference is likely due to the differences in the style of internal feeds used and the fact that the study used cylindrical holes instead of shaped. The causes of this difference are investigated further in section 3.3.2.

Next, a plot of laterally averaged ϕ values is presented to better compare between plenum and impingement.

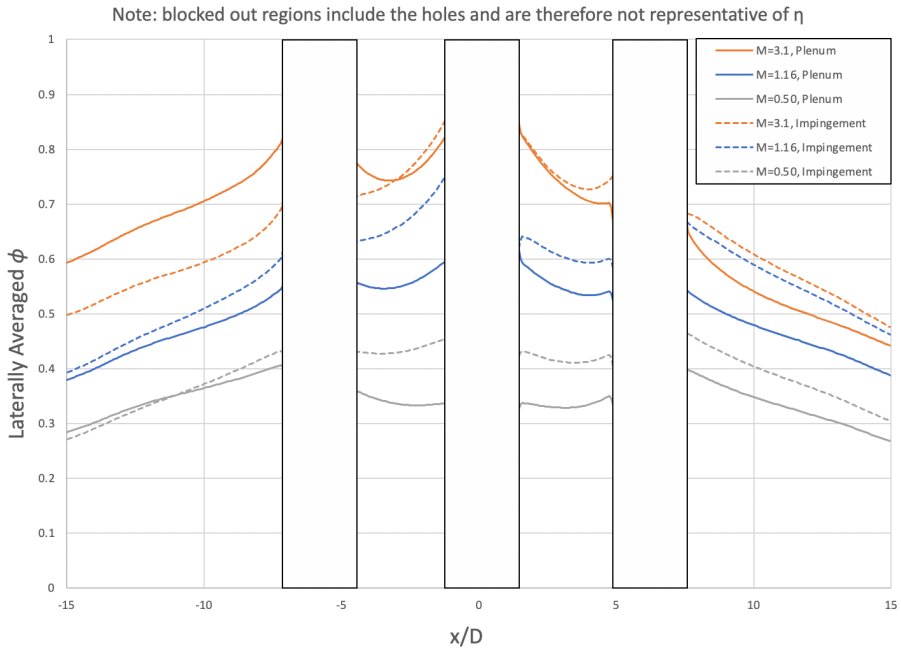

Figure 3.24: Laterally Averaged Overall Effectiveness for Plenum and Impingement Feeds

This plot again shows the higher performance downstream of the pressure side hole for the plenum feed and downstream of the suction side hole for the impingement feed. It also shows the similarity between feeds at $M = 3.1$ in the region between the outer holes (-5D to 5D), and the greater performance of the impingement feed in this region for $M = 1.16$ and $M = 0.50$.

Overall, it appears the impingement feed makes a significant impact on leading-edge internal cooling for $M = 1.16$ and $M = 0.50$, but it is difficult to tell if it makes a

significant impact at $M = 3.1$ due to the extensive difference in film cooling at this blowing ratio.

3.3.2 Heat Flux and Heat Transfer Contours

To better see the feed effects on internal and bore convective cooling, results were gathered for the surface heat flux (q'') and heat transfer coefficients (h) inside of the blade. Heat transfer coefficients are presented alongside heat flux results to show areas where the heat flux is primarily caused by high heat transfer coefficients and areas where the heat flux is primarily due to temperature differences.

First, Figures 3.25 and 3.26 show the q'' and h values on the internal coolant chamber surface for the plenum and impingement feed, respectively, for all three blowing ratios. Note that the heat flux at the back of the chamber is unrealistic for a realistic, fully cooled blade. In this study, it is present because the back sections of the blade are not cooled. In an actual blade, there would generally be additional coolant chambers behind the leading-edge chamber, causing negligible heat flux on the back wall.

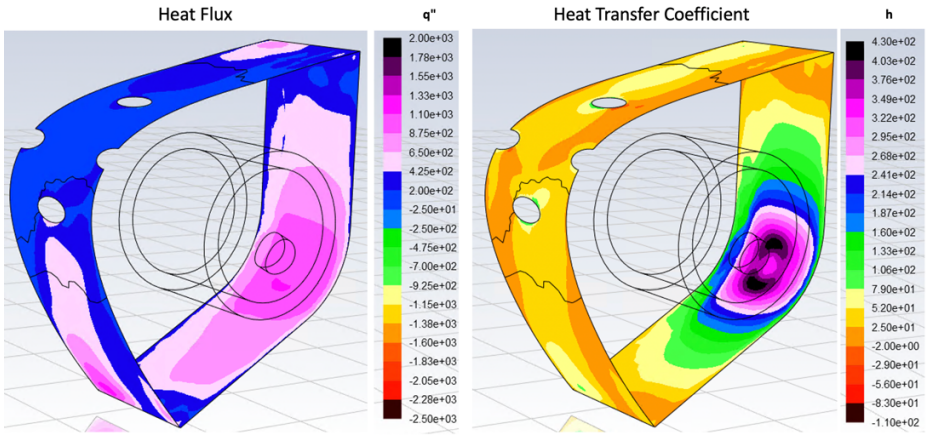

a) $M = 3.1$

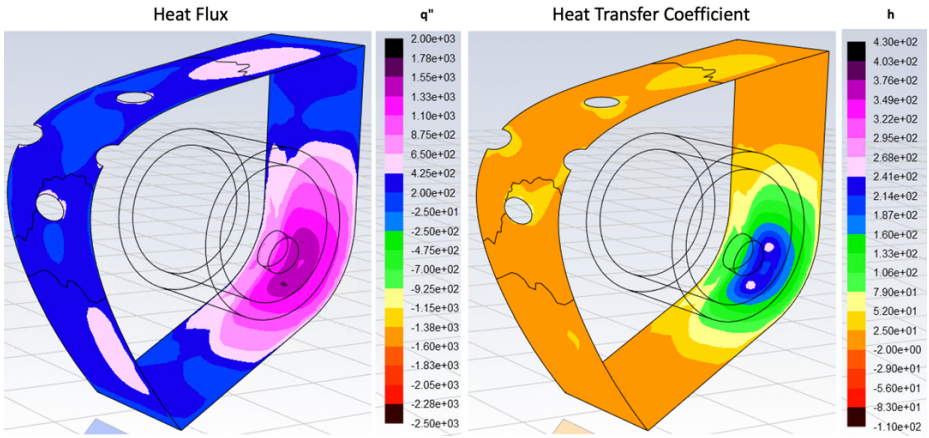

b) $M = 1.16$

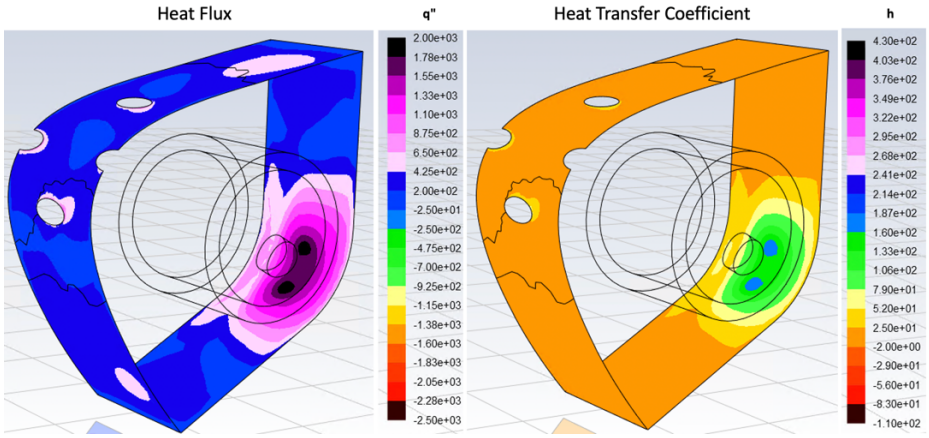

c) $M = 0.50$

Figure 3.25: Plenum Feed Internal Surface Heat Flux and Heat Transfer Coefficients

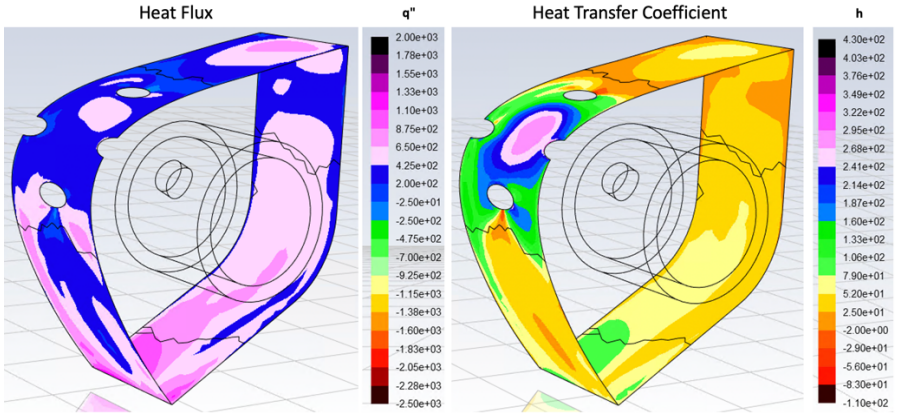

a) $M = 3.1$

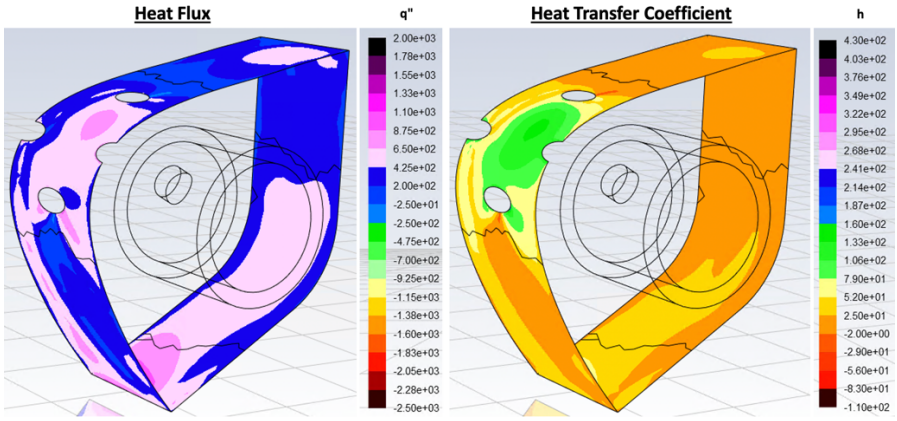

b) $M = 1.16$

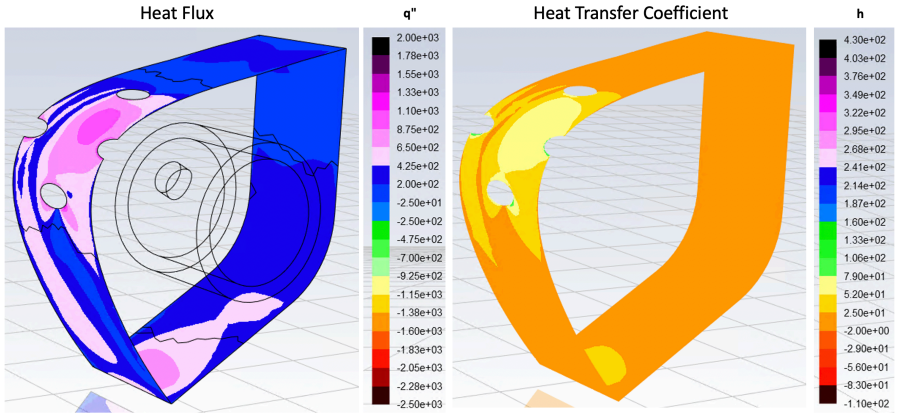

c) $M = 0.50$

Figure 3.26: Impingement Feed Internal Surface Heat Flux and Heat Transfer Coefficients

These figures show that the internal heat transfer coefficients are generally much smaller for the plenum feed than the impingement feed, which is expected due to the impact of the impingement feed on the internal flow fields. Also as expected, the exception is the back surface of the chamber where the plenum coolant jet impinges, causing high heat transfer coefficients. As mentioned above, the heat flux on this back surface is very high for the plenum but would be much smaller for a realistic fully cooled turbine blade which would have more coolant chambers behind the leading-edge chamber.

For the impingement feed, the coolant impinging on the leading edge predictably causes high heat transfer coefficients, especially at higher blowing ratios. However, the heat flux at the back of the leading edge is smaller at higher blowing ratios and increases as blowing ratio decreases. The decrease in heat flux, as M and h increase, indicates a significant decrease in temperature difference as the blowing ratio increases. This can be attributed to an increase in film cooling adiabatic effectiveness and bore cooling in the holes, and explains the ϕ similarity at $M = 3.1$ for the region between the outer holes. At the two lower blowing ratios, the film cooling is not as significant, so the high heat transfer coefficients caused by the impingement feed lead to higher heat flux and thus more effective overall cooling of the leading edge.

Next, the effects of the feeds on in-hole bore cooling are examined. To quantify the percentage of convective cooling due to bore cooling and due to internal cooling, tables 3.1 and 3.2 show the total heat transfer rate through the surfaces of all three holes (bore cooling) and through the entire internal chamber surface for the plenum and impingement

feed, respectively. The tables also show the percentage of total convective cooling comprised by the cooling through these surfaces.

M	Bore Cooling Heat Transfer Rate (W)	% of Total Convection	Internal Cooling Heat Transfer Rate (W)	% of Total Convection
3.1	1.56	36.0%	2.77	64.1%
1.16	1.64	39.0%	2.58	61.2%
0.50	1.21	33.9%	2.35	66.1%

Table 3.1: Plenum-Fed Bore and Internal Cooling

M	Bore Cooling Heat Transfer Rate (W)	% of Total Convection	Internal Cooling Heat Transfer Rate (W)	% of Total Convection
3.1	1.30	30.2%	2.99	69.8%
1.16	1.32	34.8%	2.48	65.2%
0.50	1.14	35.6%	2.07	64.4%

Table 3.2: Impingement-Fed Bore and Internal Cooling

The tables show that the plenum feed leads to more bore cooling and less internal cooling, as expected given the higher internal heat transfer coefficients caused by the impingement feed. Interestingly, the plenum has the greatest bore cooling at $M = 1.16$, likely because it does not lead to as much internal cooling as at $M = 3.1$, but the coolant is not heated as much before entering the holes as for $M = 0.50$. For the impingement feed, the bore cooling percentage increases as blowing ratio decreases, since the heat transfer coefficients due to the impingement jet decrease, causing less internal cooling. It should also be noted that the actual internal cooling is likely unrealistically high, since the areas behind the leading edge in a real blade would be colder, leading to less heat transfer at the back of the chamber.

Overall, the impingement feed affects leading-edge internal and bore cooling in different ways depending on the blowing ratio. At $M = 3.1$, the higher internal cooling caused by the impingement feed is offset by the higher bore cooling of the plenum case, leading to similar convective cooling between the two feeds. However, the film cooling dominates for this blowing ratio so the overall effectiveness is still significantly different between feeds. At $M = 1.16$, the film cooling is more similar between the plenum and impingement case, but in this case the increase in h caused by the impingement jet causes higher overall cooling for the impingement feed. This is despite the fact that the bore cooling is higher for the plenum case at this blowing ratio, meaning the internal cooling caused by the impingement jet is even higher than this bore cooling increase. The $M = 0.50$ case is similar to the $M = 1.16$ case, with less bore cooling for both feeds caused by increased heating of the coolant before reaching the holes. Because the bore and film cooling is low for this case, the internal cooling caused by the impingement jet leads to better overall leading-edge film cooling. It should however be noted that the high heat flux on the back of the chamber for the plenum case may have significantly affected the bore cooling by heating the coolant. Because this back wall heat flux is not realistic for an actual blade model, the overall cooling results for the plenum feed are questionable.

Chapter 4: Conclusion[4]

In this study, RANS CFD simulation was used to analyze the internal flow fields feeding showerhead film cooling holes on the leading edge of a blade and how they affect the cooling performance. While the simulation results proved to have some limitations, they showed many strong similarities to experimental results. These results show that RANS simulation can effectively capture most of the important physics associated with the flow fields in turbine blade leading-edge cooling, and is therefore a viable tool to analyze the internal flow fields present in these configurations when experimental methods cannot.

Using these computational simulations, the reasons that the impingement-fed configuration performed differently than the plenum-fed configuration were determined. Ultimately, the key factor was the rotation in the holes caused by the flow from the impingement jet hitting the inner surface and entering the holes at an angle. This rotation was beneficial in the suction side and stagnation row holes, causing the main coolant jet to exit the holes in locations which improved performance compared to the plenum-fed case. In contrast, the plenum-fed holes had little rotation within the holes and the coolant jets exited the holes near the top of the hole outlet for all three hole locations. However, it was observed that the impingement jet negatively affected the flow through the pressure side hole for $M = 3.1$ by skewing the jet even more towards the top of the hole and decreasing spreading in the diffuser section compared to the plenum case. It should be noted that the performance of the pressure side hole for the plenum case at $M = 3.1$ did

[4]Includes material previously published in:
Easterby, Christopher C, Moore, Jacob D and Bogard, David G. "CFD Evaluation of Internal Flow Effects on Turbine Blade Leading-Edge Film Cooling with Shaped Hole Geometries." *Proceedings of the ASME Turbo Expo*. GT2021-59780. Online, June 7–11, 2021.
The author of the current thesis was the lead author for this paper.

not agree well with experimental results, so the validity of computational predictions for this case is questionable.

It was also observed that the impingement feed sometimes had a significant impact on the convective cooling of the leading edge. At the highest blowing ratio, the decrease in bore cooling caused by the impingement jet heating the coolant, along with the fact that film cooling dominated, meant that the impingement feed did not significantly impact overall cooling. However, at the lower two blowing ratios, the increase in internal heat transfer coefficient caused by the impingement jet was more impactful than the film cooling and bore cooling, leading to better overall cooling. It was also noted that heat flux at the back of the chamber caused by the unrealistically high temperature of the downstream blade region may have had a negative impact on the accuracy of the overall plenum-fed cooling results.

Several future studies are suggested to build on the ideas of this thesis. First, an investigation into why the plenum-fed $M = 3.1$ pressure side hole was predicted poorly could be very informative for RANS leading-edge film cooling modelling. Next, while no holes saw the coolant jet exiting exactly at the bottom of the hole or on the downstream side of the hole, it is speculated that a rotation which caused this could lead to even better performance, as the jet would likely stay attached even more effectively. Future work that looks at the sensitivity of the flow fields to where the impingement jet hits the inner surface could provide insight into how to achieve these ideal flow fields, while a study which seeks to optimize the internal feed for film cooling performance could be even more beneficial. A study which looks to optimize the internal feed for overall film cooling would also be useful, and the optimized overall cooling feed would be interesting to compare with the results for the optimal film cooling feed.

Overall, the study concludes that the internal feeds in leading-edge film cooling can significantly impact the flow through the holes and thus the film cooling performance and overall cooling performance. While this paper only focused on two variations of the same design, the internal flow field analysis presented may be applied to a number of different feed and showerhead designs. The results differ in some ways from experimental results, but the effectiveness of RANS in modelling almost all of the expected flow fields presents RANS CFD as a feasible way of explaining internal feed effects seen in experimental studies, which the present study suggests may be very significant.

References

[1] Bogard, D. G. and Thole, K. A. "Gas Turbine Film Cooling." *Journal of Propulsion and Power* Vol. 22 No. 2 (2006): pp. 249-270.

[2] Moore, Jacob D., Easterby, Christopher C. and Bogard, David G. "Experimental and Computational Investigation of External Flowfield and Film Cooling Performance Effects Due to Impingement Coolant Feed in the Leading Edge of a Turbine Blade." *Proceedings of the ASME Turbo Expo*. GT2021-60015. Pittsburg, PA, USA, June 7–1, 2021.

[3] Reiss, H. and Bölcs, A. "Experimental Study of Showerhead Cooling on a Cylinder Comparing Several Configuration Using Cylindrical and Shaped Holes." *J. Turbo-mach.* Vol. 122 No. 1 (2000): pp. 161–169.

[4] Gao, Zhihong and Han, Je-Chin. "Influence of Film-Hole Shape and Angle on Shower-Head Film Cooling Using PSP Technique." *Journal of Heat Transfer* Vol. 131 No. 6. (2009): DOI 061701.

[5] Moore, Jacob D. "Systematic Study of Shaped-Hole Film Cooling at the Leading Edge of a Scaled-Up Turbine Blade." Ph.D. Thesis, The University of Texas at Austin, Austin, TX. 2020.

[6] Mouzon, Brian D, Terrell, Elon J, Albert, Jason E and Bogard, David G. "Net Heat Reduction and Overall Effectiveness for a Turbine Blade Leading Edge." *Proceedings of the ASME Turbo Expo 2005*: pp. 825–832. 2005.

[7] Ravelli, Silvia, Dobrowolski, Laurene and Bogard, David G. "Evaluating the Effects of Internal Impingement Cooling on a Film Cooled Blade Leading Edge." *Proceedings of the ASME Turbo Expo 2010*: pp. 1655–1665. 2010.

[8] Ravelli, S. and Barigozzi, G. "Comparison of RANS and Detached Eddy Simulation Modeling Against Measurements of Leading Edge Film Cooling on a First-Stage Vane." *Journal of Turbomachinery* Vol. 139. (2017): DOI 10.1115/1.4035161.

[9] Zhang, Mingjie, Wang, Nian, Chen, Andrew F. and Han, Je-Chin. "Influence of Turbine Blade Leading Edge Profile on Film Cooling with Shaped Holes." *Journal of Thermal Science and Engineering Applications* Vol. 10. (2018): DOI 10.1115/1.4039703.

[10] Kopriva, James E. “The Role of Free-Stream Turbulence on High Pressure Turbine Aero-Thermal Stage Interaction.” Ph.D. Thesis, Northeastern University, Boston, MA. 2017.

[11] Jones, Fraser B. “Investigation of Inlet and Diffuser Geometry Modifications on Film Cooling Performance of Additively Manufactured Shaped Holes in Crossflow.” Ph.D. Thesis, The University of Texas at Austin, Austin, TX. 2020.

[12] Town, Jason, Straub, Douglas, Black, James, Thole, Karen A. and Shih, Tom IP. “State-of-the-Art Cooling Technology for a Turbine Rotor Blade.” *Journal of Turbomachinery*, 140(7):071007, 2018.

[13] Christian Saumweber and Achmed Schulz. “Effect of Geometry Variations on the Cooling Performance of Fan-Shaped Cooling Holes.” *Journal of Turbomachinery*, 134(6), 2012.

Vita

Christopher Easterby was born in Houston, TX in 1996 and lived there until moving to Austin to attend UT in 2015. He received a B.S. in mechanical engineering from UT in 2019, along with a certificate of computational engineering and science. He stayed at UT for graduate school and received a M.S.E. in mechanical engineering with a focus on thermal fluid systems in 2021. He now plans to enter the workforce with a focus on thermal fluid system research.

Email: cceasterby@utexas.edu

This thesis was typed by Christopher Easterby